

MONITORING AQUATIC HABITAT RESTORATION  
USING MULTISPECTRAL HIGH-RESOLUTION REMOTE SENSING

by

DANIEL RYAN BALDWIN

A THESIS

Presented to the Department of Geography  
and the Graduate School of the University of Oregon  
in partial fulfillment of the requirements  
for the degree of  
Master of Science

June 2019

THESIS APPROVAL PAGE

Student: Daniel Ryan Baldwin

Title: Monitoring Aquatic Habitat Restoration using High-Resolution Multispectral Remote Sensing

This thesis has been accepted and approved in partial fulfillment of the requirements for the Master of Science degree in the Department of Geography by:

Patricia McDowell                      Chairperson

Mark Fonstad                              Member

and

Janet Woodruff-Borden              Vice Provost and Dean of the Graduate School

Original approval signatures are on file with the University of Oregon Graduate School.

Degree awarded June 2019

© 2019 Daniel Ryan Baldwin

## THESIS ABSTRACT

Daniel Ryan Baldwin

Master of Science

Department of Geography

June 2019

Title: Monitoring Aquatic Habitat Restoration using Multispectral High-Resolution Remote Sensing

The restoration of riverine habitats is a widespread industry valued at millions of dollars annually. Quantifying the success of river restoration projects is an important component of restoration planning but is often impractical in the long term. This study uses cheaply available consumer grade technology to monitor a restoration site on the Middle Fork John Day River, Oregon, and evaluate changes using 3 sets of high-resolution imagery over a 12-year period. Additionally, it explores the experimental generation of submeter resolution NDVI imagery through a modified consumer grade camera. This study finds that restoration is moving towards its intended goals. Riparian vegetation has generally expanded and encroached on the channel within the study site, and that the most vigorous vegetation is that which has been protected from deer and elk browse in addition to cattle grazing removal. Wood structures have remained relatively stable.

## CURRICULUM VITAE

NAME OF AUTHOR: Daniel Ryan Baldwin

### GRADUATE AND UNDERGRADUATE SCHOOLS ATTENDED:

University of Oregon, Eugene

### DEGREES AWARDED:

Master of Science, Geography, 2019, University of Oregon  
Bachelor of Science, Environmental Studies, University of Oregon, 2017

### AREAS OF SPECIAL INTEREST:

Fluvial Geomorphology and Ecological Restoration

High-Resolution Remote Sensing

### PROFESSIONAL EXPERIENCE:

Habitat Monitoring Technician, The Freshwater Trust, 2017 - 2019

### GRANTS, AWARDS, AND HONORS:

William G. Loy Award for Excellence in Cartography, "Selected Indigenous Names of Northwest Mountain Peaks", University of Oregon, 2019

## ACKNOWLEDGMENTS

I wish to express sincere appreciation to Professors Pat McDowell and Mark Fonstad for all of their support, both in the production of this manuscript, and in my development as an academic. I want to thank Pat for introducing me to the field of fluvial geomorphology and teaching me how to look at landscapes critically, and Mark for introducing me to a host of remote sensing methodologies that have been invaluable throughout this process. I would also like to thank the Confederated Tribes of Warm Springs for allowing me access onto their beautiful property on the Middle Fork John Day River, and to the Middle Fork John Day Intensely Monitored Watershed for providing valuable monitoring and historical information about my study sites. I'd also like to thank the University of Oregon Department of Geography for support in conference travel and attendance, which greatly helped me hone in on my research interests.

Lastly, I would like to thank my fellow graduate students for their support, especially to current and former river research group students for their help and encouragement, along with their technical assistance along the way.

## TABLE OF CONTENTS

Chapter	Page
I. INTRODUCTION AND BACKGROUND .....	1
River Restoration in the Pacific Northwest .....	1
Challenges to Effectiveness Monitoring.....	3
Remote Sensing and Rivers .....	4
Study Site.....	5
Research Questions.....	7
II. PRODUCTION, CALIBRATION, AND TESTING OF A MULTISPECTRAL SYSTEM FOR A SMALL DRONE USING OFF THE SHELF, CONSUMER GRADE COMPONENTS .....	10
Camera Modification .....	10
Radiometric Calibration.....	13
Performance and Imagery Products .....	18
III. FIELD METHODS & IMAGE PROCESSING .....	19
Planning and Implementing UAV Flights .....	19
Structure-from-Motion Image Processing .....	21

Chapter	Page
IV. GIS ANALYSIS .....	26
Greenline Digitization.....	26
Vegetation Classification .....	29
NDVI Analysis.....	31
Large Woody Debris Assessment.....	33
V. RESULTS .....	33
Greenline.....	36
Landcover Composition.....	39
Vegetation Vigor.....	42
Large Woody Debris.....	45
VI. DISCUSSION OF RESULTS .....	50
Vegetation and LWD Monitoring.....	50
Floodplain Mapping.....	51
NDVI Performance .....	55
VII. CONCLUDING COMMENTS.....	57
REFERENCES CITED.....	59



## LIST OF FIGURES

Figure	Page
1. Hypsometric shaded relief map of the Middle Fork John Day river .....	6
2. Oxbow Conservation Area before and after restoration .....	8
3. Sensitivity curves of a typical CCD array, showing NIR wavelengths blocked by the hot mirror .....	11
4. Transmissivity of the NIR-Pass Filter.....	11
5. Example of unprocessed JPEG images taken with the Phantom III Pro FC300X camera and modified Canon A480. ....	12
6. Spectral reflectance curve of each calibration panel.....	15
7. Plot of DN's and Reflectance values for each sensor waveband used to generate calibration regression equations.....	18
8. Final RGB orthophoto generated for Oxbow Conservation area showing amount of image overlap throughout the study area.....	24
9. Orthophotographs of each band showing ground control points used for georectifying 2018 imagery to 2013 imagery.....	25
10. Greenline location examples under bankfull conditions, low flow conditions, and areas of erosion and/or incision.....	24
11. Greenline location in 2013 and 2018 .....	28
12. Example of fully digitized greenlines showing transects and points of intersection for each year's greenline .....	29
13. Example of classified imagery in Oxbow Conservation Area.....	30

Figure	Page
14. Subset of NDVI imagery focusing on restored portion of Granite Boulder Creek .....	32
15. Change in greenline to greenline width, 2006 – 2018 .....	37
16. Hotspots of greenline change.....	37
17. Change in distance from greenline to channel centerline separated into left bank and right bank, organized by time interval.....	38
18. Map results of supervised classification within Oxbow Conservation Area .....	40
19. Histograms of NDVI values for contrasting areas .....	42
20. NDVI map of oxbow conservation area .....	43
21. Subset of Forrest NDVI map .....	45
22. Downstream abundance of LWD organized by year.....	46
23. Examples of wood movement within the study area .....	47
24. Change in LWD distribution between 2013 and 2018.....	49
25. Vector floodplain map generated from field surveys showing dominant species .....	53
26. Example of supervised classification outputs from drone imagery .....	54
27. Example of shadow effects from tall Ponderosa pine trees in NDVI map .....	56

## LIST OF TABLES

Table	Page
1. UAV and Field-Based Monitoring Techniques in Oxbow Conservation Area .....	9
2. Manufacturer specifications for Phantom 3 Pro Camera and Canon A480.....	14
3. Weighted and Unweighted Mean Reflectance of Calibration Targets .....	16
4. Weighted Mean Reflectance and DN of Calibration Targets for Each Sensor Waveband .....	17
5. Flight Characteristics and JPEG Image Resolution collected by Study Site .....	20
6. Summary of Raw Data Formats and Analysis .....	35
7. Percent Composition of Land Cover Classes by year.....	39
8. Change Matrix of Classified Pixels .....	41

CHAPTER I  
INTRODUCTION AND BACKGROUND

**River Restoration in the Pacific Northwest**

In the western United States, mitigating the degradation of freshwater habitat through restoration is a longstanding priority among land managers (Palmer et al, 2005). In Fiscal Year 2015 alone, Bonneville Power Administration (BPA) reported a total of \$124 million dollars spent on improving habitat for anadromous fish in the Columbia River Basin, with an additional \$82 million spent on researching, monitoring, and evaluating these projects (NW Power & Conservation Council, 2016). Despite decades of costly habitat restoration in the Pacific Northwest, the specific ecological benefits associated with a given project in the long term are often unclear (Bennett et al., 2016). Effectiveness monitoring is critical for assessing restoration projects because it informs the adaptive management principles that guide emerging restoration techniques. Widespread effectiveness monitoring, however, is often impractical due to constraints of cost, time, and available technology (Rumps et al 2007). Industry demand for low cost alternatives to standard monitoring techniques is therefore growing. Recent technological advances in unmanned aerial vehicles (UAV) present an opportunity to improve monitoring and evaluation of river restoration projects through imagery-based reach-scale assessment. Structure from Motion (SfM) digital photogrammetry has allowed for, in contrast to infrequent and costly LiDAR surveys, the rapid and low-cost generation of high-resolution aerial imagery and DEMs of river environments using off the shelf consumer grade equipment (Fonstad 2013, Marteau 2017). This research seeks to

investigate the utility of using SfM-derived imagery to monitor river restoration by testing it in an applied habitat monitoring context with a set of practitioner-defined management goals.

Riparian vegetation is an important component of fluvial systems because of its demonstrated ability to reduce instream temperatures by shading the channel, decrease turbidity by improving bank cohesion, and influence channel morphology by supplying woody debris and increasing roughness (Corenblit et al., 2009, Kalny et al., 2017).

Riparian zones are known to play a crucial role in maintaining biodiversity and ecosystem functions, due in large part to their connecting terrestrial and aquatic systems (Beechie et al. 2010), and can be particularly sensitive to anthropogenic impacts. In the Pacific Northwest, these impacts are often related to mining, grazing, or dam construction (Bennett et al., 2016). The hydrologic connectivity a stream maintains with its surrounding floodplain can have dramatic effects on local biodiversity as well as reach-scale and watershed-scale processes. A river is considered to be “connected” with its floodplain if peak flows are likely to create flooding on a regular basis, which in turn tends to raise groundwater and support diverse plant and animal communities. Sedges (*Carex sp.*) and willows (*Salix sp.*) are considered to be generally good indicators of hydrologic connectivity between channels and banks (Winward, 2000) and can respond rapidly to grazing removal (McDowell & Magilligan, 1998; Hough-Snee et al., 2013). Floodplains with high degrees of hydrologic and biologic connectivity provide a wealth of ecosystem services, such as improving water quality, decreasing nitrate and phosphorus concentrations, maintaining biodiversity, and reducing bank erosion (Lyons

et al. 2000; Muller et al. 2015). The maintenance or enhancement of these conditions is a frequent goal of restoration throughout the region.

### **Challenges to Effectiveness Monitoring**

The diverse processes inherent to riverine habitats fundamentally require effectiveness monitoring methodologies equipped to assess both biotic and abiotic aspects of the system. Substrate monitoring has long required labor-intensive manual counts of clasts (e.g., Wolman 1954) which, despite improvements in remote-sensing based photosieving (e.g., Vásquez-Tarrío et al., 2017), remain the standard in many studies of turbid streams where a clear view of the bed is not possible. Reach- or site-scale vegetation data is frequently collected via transect or point-based survey methods that identify species, height classes, and record browse effects (e.g., Winward, 2000; Göthe et al., 2016) Large woody debris is commonly monitored via photopoints (Roni, 2018), or with simplified inventorying that assesses abundance per channel unit length. These techniques still retain value despite new technological developments, although for cheaply available monitoring, the amount of labor required often make these techniques cost prohibitive, resulting in a shortage of long-term data.

The shortage of long term-effectiveness monitoring is well-known in restoration ecology literature (Gonzalez et al., 2015, Roni 2018), and that which does exist is met with the significant methodological challenges. While multiple scales of monitoring programs exist and may be occasionally implemented with large-scale coordination, scalar mismatches can occur between the target process being restored and the metrics chosen for evaluating the success of a given project (Knighton, 1998, Beechie et al.,

2010). For example, Bonneville Power Administration's Columbia Habitat and Monitoring Program (CHaMP), which aimed to characterize restoration throughout the Columbia watershed, was evaluated in 2018 as underrepresenting the value of tributary restoration actions (Rosgen et al, 2018). Intensively monitored watersheds (IMWs), by contrast, attempt to gauge the physical and biological response of particular watersheds to inform practices elsewhere, building on detailed site-level effectiveness monitoring to estimate watershed-level response. This is particularly crucial when examining the response of mobile organisms, e.g., salmon, to extensive changes in land use. Within the Columbia watershed, there is ample room to bridge the multiple scales of monitoring that can be facilitated by emerging remote sensing methodologies.

### **Remote Sensing and Rivers**

Rivers have long been an important area of study in remote sensing. Multispectral studies of rivers have examined in-channel units (Marcus and Fonstad, 2008), bathymetry (Dietrich 2017), and riparian zones (Jeong et al., 2016), among a host of other applications (see Bizzi et al., 2015). Structure-from-Motion (SfM) photogrammetry has recently given researchers and practitioners the ability to obtain very high-resolution imagery ( $<0.1\text{m}^2$ ) of riverine landforms with unprecedented ease (Fonstad et al., 2013). When mounted on an unmanned aerial vehicle (UAV), consumer-grade cameras are now capable of producing continuous georeferenced imagery through SfM workflows, which lends itself to continua of data, rather than traditional broad scale classification (Woodget 2017, Passalacqua et al., 2015). A continuum in this context refers to a coherent whole of data - more practically, a high resolution orthophoto and DEM that can be customized to

fit the particular needs of a survey. High-resolution UAV data have the potential to act as objective and cost-effective alternatives to traditional monitoring.

### **Study Site**

This study focuses on the Middle Fork of the John Day River (MFJD) in northeastern Oregon (Figure 1). The MFJD is one of three major headwaters of the John Day River, which is itself the longest undammed tributary of the Columbia River. The MFJD provides critical spawning habitat for wild native runs of spring Chinook and summer steelhead salmon. This river drains 2088 km<sup>2</sup> of semi-arid mountainous terrain receiving between 25cm and 100cm of precipitation annually, with a range of elevation of 2500m at its headwaters to 670m at its confluence with the North Fork John Day. The MFJD additionally has a long history of human impacts, the most dramatic of which is the floodplain dredge mining that occurred during the late 19<sup>th</sup> through mid-20<sup>th</sup> century (Middle Fork IMW, 2017, Magilligan & McDowell, 1998). Grazing pressure, and manual clearing additionally stripped much of the floodplain of its woody vegetation, increasing the solar loading on the channel and intensifying high summer stream temperatures that threaten cold water dependent salmon. In dredged reaches, the mainstem MFJD became incised and disconnected from its floodplain. Additionally, the coarse cobble-sized substrates left by dredging prevented already degraded reaches from meandering naturally – a pattern seen across many streams in the American West (Kondolf, 1997).

Since the 1990s, extensive habitat restoration has been done to improve conditions for ESA listed aquatic species, with a mix of passive and active techniques that vary in intensity throughout the watershed. The goals of these projects were generally to decrease summer water temperature, decrease turbidity, and, in actively



restored sites, to reduce the slope and velocity of the channel (Middle Fork IMW, 2017). The Middle Fork John Day's patchwork of restoration techniques, as well its status as an Intensively Monitored Watershed makes it an ideal place for a methods test, as numerous studies have been conducted on restoration effectiveness within this watershed (Middle Fork IMW, 2017).

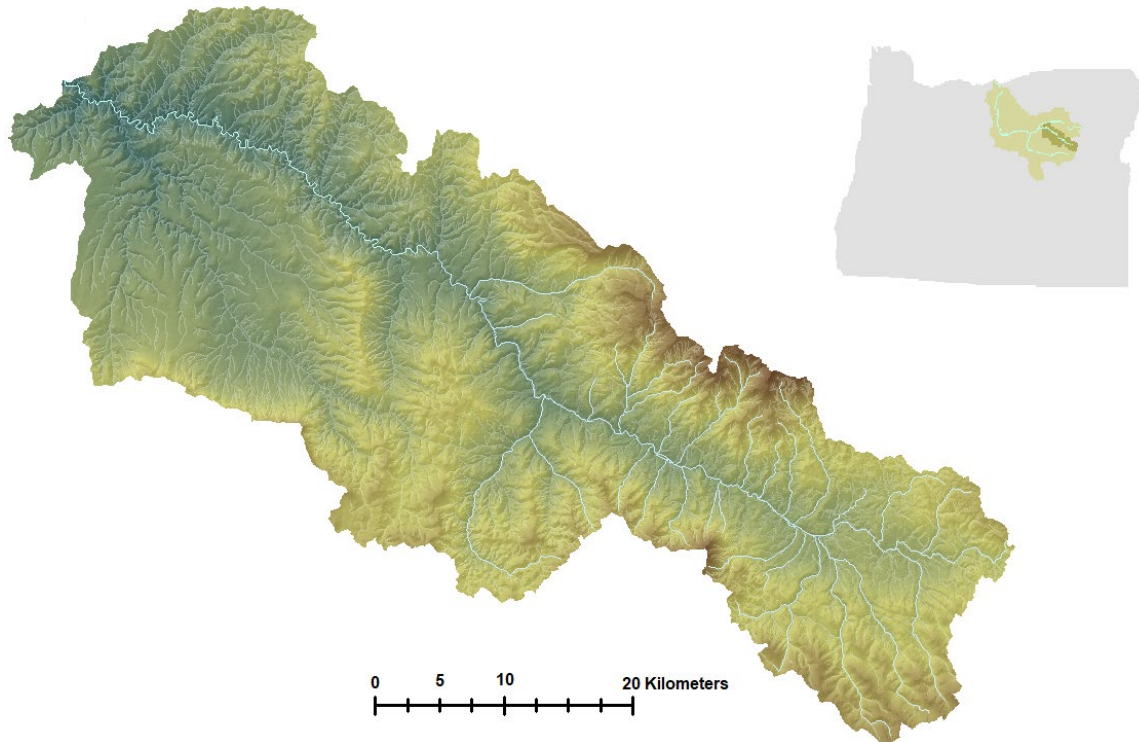


**Figure 1:** Hypsometric shaded relief map of the Middle Fork John Day river showing its position within the John Day watershed

The data collected for this study are within two conservation areas in the upper MFJD. The first, Oxbow Conservation Area, was acquired by the Confederated Tribes of Warm Springs (CTWS) in 2001 and underwent extensive restoration in five phases between 2011 and 2015 to undo the effects of gold dredging in the 1940s. Prior to restoration at Oxbow, the channel was artificially bifurcated by dredging, with a straight, badly incised northern channel left behind by the dredge diverting much of the flow from

the relatively intact meandering southern channel (see Figure 2). Forrest Conservation Area is several kilometers upstream and was also purchased by CTWS in 2001 – this reach underwent multiple phases of restoration in the same time period, the most recent of which focuses on removing boulder weirs from a previous generation of work and replacing them with large woody debris jams. In addition to LWD placement, extensive strips of riparian vegetation were planted near the channel to increase stream shade and, in the future, provide more large wood to the channel.

### **Research Questions**

This research aims to characterize variables that, while specific to the goals of restoration in this watershed, are often are of interest in long-term effectiveness monitoring programs. While numerous proof-of-concept studies have demonstrated the ability of drone imagery to inexpensively characterize meso- and micro-scale river habitats (e.g. Marteau 2017, Dietrich 2016), less work has been done in extracting and assessing explicit monitoring data from this imagery in an applied habitat restoration context, particularly with a high-resolution multispectral approach. Table 1 gives a complete list of the variables examined in Question 1, as well as their field-based equivalents as described in the Maintenance and Monitoring Plans for the MFJD.

**Question 1:** How can key UAV-derived monitoring variables be used to assess restoration performance within this study reach?

**Question 2:** How do observed changes present within Oxbow Conservation Area align with goals of restoration for the Middle Fork John Day?



**Figure 2:** Oxbow Conservation Area before restoration (left) and after restoration (right). Following restoration, the northern dredge channel has been eliminated and a new channel has been constructed for Granite Boulder Creek, in addition to multiple grazing exclosures, large woody debris placement, and riparian plantings.

**Table 1** | UAV and Field-Based Monitoring Techniques in Oxbow Conservation Area

<i>Restoration Objective</i>	<i>Restoration Actions</i>	<i>UAV-Derived Variable</i>	<i>Traditional Monitoring</i>
Dynamically stable natural channel form	<ul style="list-style-type: none"> <li>○ Dredged northern channel sealed off, restored flow in south channel</li> <li>○ Construction of large woody debris jams</li> </ul>	<ul style="list-style-type: none"> <li>○ Greenline to greenline width by year to estimate channel migration</li> </ul>	<ul style="list-style-type: none"> <li>○ Width/depth measurements, channel lateral migration</li> </ul>
Enhance riparian vegetation	<ul style="list-style-type: none"> <li>○ Removal of livestock grazing, with additional fencing to reduce deer &amp; elk browse</li> <li>○ Riparian planting within Granite Boulder Creek and the mainstem Middle Fork John Day</li> </ul>	<ul style="list-style-type: none"> <li>○ NDVI as a correlate for vigor of plantings throughout restoration sites</li> <li>○ Areal mapping of vegetation communities using textural / spectral properties to estimate diversity</li> </ul>	<ul style="list-style-type: none"> <li>○ Vegetation plots, visual browse assessment</li> </ul>
Increased instream habitat	<ul style="list-style-type: none"> <li>○ Construction of large woody debris jams to facilitate cover and spawning gravel storage</li> </ul>	<ul style="list-style-type: none"> <li>○ Assessment counts of logjams to assess structure stability</li> </ul>	<ul style="list-style-type: none"> <li>○ Field-based structure stability count of LWD</li> </ul>

CHAPTER II  
PRODUCTION, CALIBRATION, AND TESTING OF A FOUR-BAND  
MULTISPECTRAL SYSTEM FOR A SMALL DRONE  
USING OFF-THE-SHELF-COMPONENTS

**Camera Modification**

Plant vigor is important to understand when making management decisions about revegetation projects similar to the MFJD. Multispectral methodologies that utilize non-visible wavelengths of light can provide valuable information about landscape function beyond what can be seen by the human eye (Njiland, 2012). Near infrared is particularly useful for detecting the chlorophyll present in plants, which functions as a spatial correlate for vigor and stress. A 4-band multispectral camera is a common but expensive tool to assess plant vigor in the near infrared. While many calibrated 4 band cameras are available for purchase for several thousand dollars, this study investigated the utility of using a cheaper modified Canon Powershot A480 to explore the spatial patterns of vegetation health.

Most consumer grade cameras come equipped with either charged coupled device (CCD) or complementary metal oxide semiconductor (CMOS) sensors that are sensitive to nonvisible spectra in near-infrared. CCD and CMOS sensors record the amount of red, green, and blue light that reaches a given point, effectively storing an image as a 3-band raster stack. However, what is perceived and recorded as “red”, “green”, or “blue” by the sensor fundamentally represents the sum of a range of spectra that fall outside of the

wavelengths one would normally assign to red green or blue light (Figure 3). Non-visible spectra recorded as “RGB” light will contaminate this color, resulting in an unnatural looking image. To account for this, camera manufacturers install a “hot mirror” that prevents near infrared and UV light from reaching the sensor. The result of this is a natural color image similar to what is perceived by the human eye. By removing the hot mirror and restoring the sensor’s expanded spectral sensitivity, one only needs to block the remaining red, green, blue, and ultraviolet light via a new filter for the camera to perceive *only* near infrared light. The camera will still record raster data across three “RGB” bands, but the range of wavelengths reaching the sensor will be far narrower and confined to the near infrared portion of the spectrum.

To produce a low-cost near infrared imaging instrument for this study, a Canon Powershot A480 was modified by MaxMax LLC to capture infrared images. The hot mirror was removed and a 1” diameter, lightweight plastic infrared longpass filter was subsequently installed over the camera lens to pass only light with wavelengths between 650nm and 1000nm (Figure 4). The steep transition slope of the longpass filter allows for nearly all near infrared light to be transmitted efficiently to the sensor while minimizing

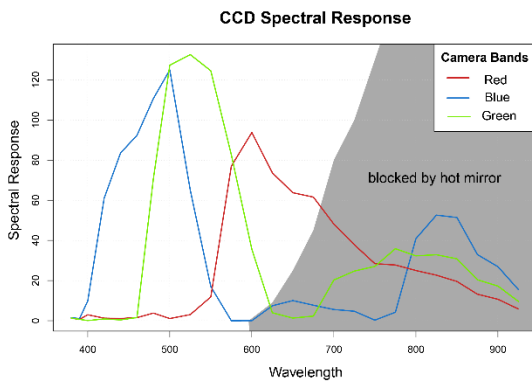


**Figure 3:** Sensitivity curves of a typical CCD array, showing NIR wavelengths blocked by the hot mirror. (Data source: Dan Lewellyn 2018)

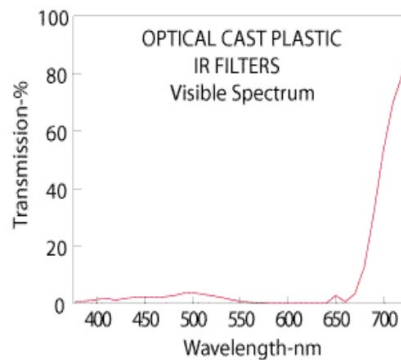


**Figure 4:** Transmissivity of the NIR-Pass Filter. (Figure Source: Edmund Optics, 2018)

the potential for visible light to contaminate the final result. The resulting images contain only near infrared radiation and can be treated as a single band similar to those produced by widely used multispectral sensors. Figure 5 shows an example of the raw aerial images produced by a standard RGB camera compared with a raw near-infrared image.

Within the range of spectral sensitivity of the Canon camera, the IR filter passes as much as 80% of near infrared light, which is sufficient for the production of aerial imagery under well-lit conditions. Because slightly more near-infrared light is captured on the red band of the Canon camera than the blue or green (Figure 3), I used only the modified red band of the camera to extract NIR data. While other studies utilize the blue band of the camera to minimize interference, the red band records comparatively more near infrared radiation than the blue, making it a practical choice in situations where the IR filter has a steep absorption curve and removes the vast majority of visible red light (see Figure 4). Additionally, the NIR sensitivity peak in the camera's blue band occurs near 850 nanometers. In vegetation applications, the "red edge" between 680nm and 730nm contains the strongest change between visible red and near infrared and is considered to be the best portion of the spectrum to emphasize in terms of spectral



**Figure 5:** Example of unprocessed JPEG images taken with the Phantom III Pro FC300X camera (left) and modified Canon A480 (right). The RGB image at the left can be subsequently broken down into its 3 constituent bands of visible light and merged with the NIR image to produce a 4-band raster stack.

indices (Tucker 1979). The total cost to produce a drone-capable NIR sensitive camera came to \$160: \$125 for the removal of the hot mirror, \$25 for the camera, and \$10 for the longpass filter. A standard drone-mounted NIR-sensitive camera, by contrast, can cost upwards of \$3,000.

To allow for the use of an intervalometer and optimized remote sensing settings, the KAP (Kite Aerial Photography) Exposure Control script was installed on the camera's memory card. KAP Exposure Control is an open source Canon Hack Development Kit (CHDK) script designed for situations in which the camera is in constant motion. The intervalometer included in the script allows the camera to take pictures at a predefined interval, making it useful for drone mounted photography in situations where the camera cannot be remotely controlled. Additionally, the script allows the user to store predetermined settings which need to be recorded for calibration purposes. Flight details are provided and discussed in detail in Section VI, part i.

### **Radiometric Calibration**

Because of the different physical properties of the two cameras, radiometric calibration is necessary to produce the 4-band imagery stacks needed for indices (Mathews, 2015). The simplified empirical line calibration method used by Wang and Myint (2015) provides a practical and effective method to convert the digital numbers (DNs) of two different cameras to reflectance, such that they can be quantitatively comparable. Manufacturer specifications for both the DJI Phantom Pro III FC300X camera and modified Canon are detailed in Table 1 below.



**Table 2** | Manufacturer specifications for Phantom 3 Pro Camera and Canon A480

<i>Camera Model</i>	<i>Lens IFOV</i>	<i>Sensor Size:</i>	<i>Effective Pixels</i>	<i>Image Size</i>
DJI FC300X	94°	6.17 x 4.55mm	12.4 megapixels	4000 x 3000px
Canon Powershot A480	82.7°	6.17 x 4.55mm	10.0 megapixels	3648 x 2736px

For this study, I optimized the settings of each camera for the sunny conditions typical of late summer in the Middle Fork John Day. The Phantom III Pro camera was programmed with a shutter stop of 1/2500 sec, f-stop of f/2.8, and ISO of 400. Using the CHDK script described in section i., the Canon was set with a constant shutter speed of 1/2000 sec, f-stop of f/3, and ISO of 800. The high ISO setting on the Canon is necessary as a result of the smaller amount of light reaching the sensor - as the longpass filter allows the camera to “see” roughly 1/3 of the radiation that simultaneously reaches the Phantom camera’s sensor.

Numerous past studies utilizing the empirical line calibration method (See Mathews et al., 2015, Berra et al., 2017) have used a single material at various brightness levels, or simply one very light and one very dark panel (Smith & Milton, 1999). This may not, however, be entirely representative of the actual spectral curves that may be encountered in imagery. To account for this, I selected calibration panels for their varied spectral curves, to better approximate diverse spectral characteristics encountered in imaging. To calibrate the images to reflectance, a FieldSpec Handheld spectrometer was used to gather the reflectance spectral curve for each panel (Figure 6). Panel 8 was discarded because its spectral curve changed significantly within the near-infrared band, resulting in an anomalously high DN in relation to its reflectance.

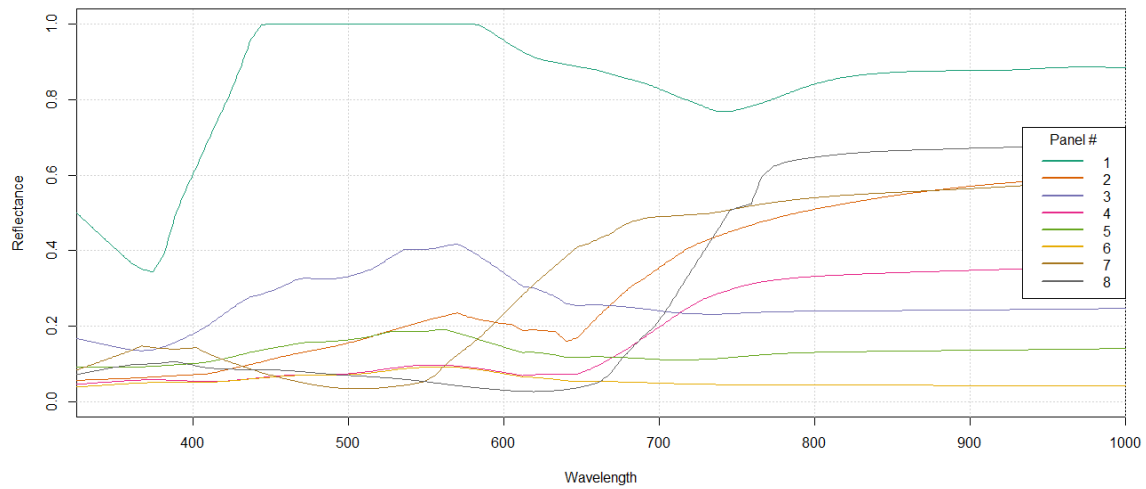


**Figure 6:** Spectral reflectance curve of each calibration panel.

Because the camera sensors are not equally sensitive to all wavelengths of light within their band (see Figure 3), producing a weighted average of reflectance is advantageous as it gives a more accurate estimate of the radiation actually being perceived by the sensor. Many studies (e.g., Coburn, 2018) utilize a simple unweighted average of the reflectance across all wavelengths within a respective band (in other words, it assumes the camera records the entire band equally), but this may mask some variation in the sensor that has the potential to affect the final raster output. For example, the red band in Figure 3 shows a strong peak at 500nm, while other wavelengths of light within the red band are far less represented. An unweighted average assumes equal sensitivity to the entire range. For each panel, the reflectance at a given wavelength (Figure 6) was weighted by spectral sensitivity in Figure 3 and summed to produce a “weighted reflectance that is more representative of the camera sensitivity using the equation:

$$\bar{r} = \sum_{i=350nm}^{950nm} (r_i * w_i)$$

Where  $\bar{r}$  is the weighted average reflectance, and  $w_i$  is the weight derived from the spectral sensitivity curves in Figure 3 for a given wavelength,  $r_i$ . After assigning weights, each mean reflectance can then be plotted against its respective blue, green, red, and near-infrared DN in their respective images taken at the same time as the spectrometer data. An important limitation of interpreting these calibrated values, particularly those in visible wavelength, lies in the difference between the sensors. The Phantom 3's FC300X utilizes a CMOS sensor, for which spectral sensitivity data was not available. Sensitivity is thus assumed to be roughly equivalent to the sensitivity of a standard CCD array.

**Table 3** | Weighted and Unweighted Mean Reflectance of Calibration Targets

<i>Band</i>	<i>Target 1 (P101)</i>		<i>Target 2 (P102)</i>		<i>Target 3 (P103)</i>		<i>Target 4 (P104)</i>	
	<i>Weighted</i>	<i>Non</i>	<i>Weighted</i>	<i>Non</i>	<i>Weighted</i>	<i>Non</i>	<i>Weighted</i>	<i>Non</i>
R	0.33	0.30	0.28	0.27	0.18	0.18	0.13	0.13
G	.29	.30	.33	.27	.35	.32	.16	.13
B	.25	.30	.30	.27	.15	.18	.15	.13
NIR	0.48	0.51	0.24	0.24	0.30	0.32	0.12	0.13

Table 3 shows the weighted and unweighted mean reflectance values for a subset of calibration panels. Though the weighted values are typically in good or full agreement with each other, they nevertheless represent a more accurate estimation of the radiation sensed by the camera.

**Table 4** | Weighted Mean Reflectance and DN of Calibration Targets for Each Sensor Waveband

<i>Band</i>	<i>Target 1 (P100)</i>		<i>Target 2 (P101)</i>		<i>Target 3 (P105)</i>		<i>Target 4 (P102)</i>	
	<i>Reflectance</i>	<i>DN</i>	<i>Reflectance</i>	<i>DN</i>	<i>Reflectance</i>	<i>DN</i>	<i>Reflectance</i>	<i>DN</i>
R	0.88	254.9	0.37	197.3	0.04	120.6	0.28	213.10
G	0.96	255	0.49	206.4	0.04	105.27	0.33	198.87
B	0.94	255	0.52	169.5	0.04	93.9	0.29	197.27
NIR	0.83	249.5	0.19	228.1	0.04	135.0	0.23	195.7

Table 4 lists a subset of calibration target DNs paired with their respective weighted reflectance used to build regression equations to convert red and near-infrared orthophotos to reflectance (Figure 7).

The  $R^2$  values for each band are relatively low compared to those obtained by Mathews et al., 2015 and Michez et al., 2016 - this is to be expected when prioritizing diverse spectral characteristics during calibration, and highlights the caution one should have when interpreting heterogeneous materials and landscapes. It is additionally important to note that the cameras must theoretically be recalibrated if the settings are to be adjusted - for example, if imaging during cloudy conditions requires a longer shutter speed for adequate brightness, then reference image DNs would need to be re-taken with camera settings used under those conditions, and subsequently plotted against calibration panel spectral curves.

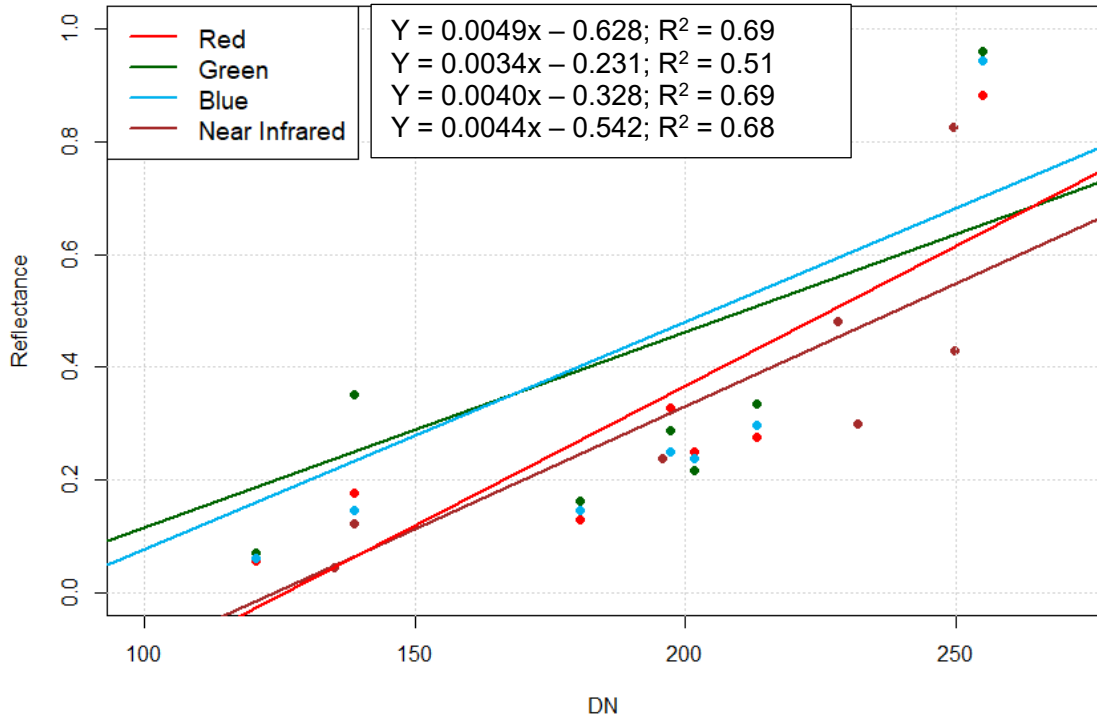


**Figure 7:** Plot of DNs and Reflectance values for each sensor waveband used to generate calibration regression equations.

## Performance and Imagery Products

The calibration regression equations pictured in Figure 7 tended to underpredict reflectance in darkest areas of imagery, resulting in negative values that are conceptually inconsistent with reflectance. This is mostly due to the lack of dark materials used during the calibration process, which was complicated by the relatively high ISO settings on both cameras. The bands within these images can thus be compared to each other since they were generated by the same calibration panels, but cannot be considered to be *spectrally* consistent with other reflectance-calibrated sources of imagery. The bands can, however, be used for false color composite imagery and indices needed for many multispectral remote sensing methods.

## CHAPTER III

### FIELD METHODS & IMAGE PROCESSING

#### **Planning and Implementing UAV Flights**

Mounting the modified Canon camera to the drone required the construction of a lightweight acrylic and carbon fiber platform. The camera mount was secured to the Phantom III frame with duct tape and positioned high enough to avoid the lens striking the ground upon landing. Both cameras were oriented 90° relative to the ground (nadir) and set to take simultaneous images at 3 second intervals. Within Oxbow Conservation Area, I collected RGB and NIR images at 30m, 50m, 100m, and 120m above ground level (see Table 5 for details). Structure from motion requires 75-80% overlap of images to allow for a given point to be imaged at minimum three times, but more overlap generally results in a more accurate end product. Excessive image overlap (>90%) has been shown to drastically increase imaging and processing time with minimal associated benefits in model quality. At all three sites, the flight plans include more overlap than is minimally necessary, since many parts of the floodplain consist of homogenous grassy vegetation and lack the strongly contrasting edges utilized by structure-from-motion algorithms.

While the Phantom III has the technical capability to image the entire floodplain at 1.5cm<sup>2</sup> or less, this can significantly increase processing time and file size, limiting the area that can feasibly be imaged and analyzed in a short amount of time. Lower resolution allows for more rapid capturing of the Earth's surface, but detail is sacrificed. Because the vegetation patches of interest are on the order of 0.5-1m<sup>2</sup>, I flew the majority

of the imagery near the Federal Aviation Administration’s maximum allowable height of 120m for consumer grade drones (FAA, 2014), at which the spatial resolution of each pixel is roughly 5-6cm<sup>2</sup>. Within Oxbow Conservation Area, the highest spatial resolution 4 band imagery (1.5cm<sup>2</sup> RGB / 1.6cm<sup>2</sup> NIR) covers approximately 1/3 of the study area and serves primarily to validate vegetation identification in comparatively lower resolution (5.4/4.8cm<sup>2</sup>) images. Table 5 summarizes the sidelap spacing, maximum flight speed, and maximum flight speed for each study site that were used to create flight plans. Marginal increases in altitude can dramatically increase the amount of area covered without significantly compromising spatial resolution. The highest resolution imagery, collected at a height of 30m within the upstream portion of Oxbow CA, has an on-the-ground footprint of 64m x 64m per raw image. By contrast, when flying at a height of 100m, the Phantom III and Canon IFOVs are capable of covering roughly 216m x 216m on the ground, meaning that a few kilometers of floodplain were readily imaged in about 4 hours of flying time.

**Table 5** | Flight Characteristics and JPEG Image Resolution collected by Study Site

<i>Study Site</i>	<i>Height Above Ground</i>	<i>Image Spacing</i>	<i>Max Flight Speed</i>	<i>Spatial Resolution</i>		<i># of Bands</i>
				<i>RGB</i>	<i>NIR</i>	
Oxbow Conservation Area	30m	20m	11.5 km/hr	1.6 cm <sup>2</sup>	1.5 cm <sup>2</sup>	4
	50m	53m	19.3 km/hr	2.7 cm <sup>2</sup>	2.4 cm <sup>2</sup>	
	100m	107m	38.6 km/hr	5.4 cm <sup>2</sup>	4.8 cm <sup>2</sup>	
	120m	120m	40.0 km/hr	6.4 cm <sup>2</sup>	5.8 cm <sup>2</sup>	
Forrest Conservation Area	30m	20m	11.5 km/hr	1.6 cm <sup>2</sup>	1.45 cm <sup>2</sup>	3
	50m	53m	19.3 km/hr	2.7 cm <sup>2</sup>	2.4 cm <sup>2</sup>	

Each flight was implemented at or near the maximum speeds for their respective heights shown in Table 5. Ground control points for this study were not collected in the field, and instead utilize a combination pseudo-invariant orthorectification from features identifiable within the floodplain and the Phantom III's direct georeferencing.

The total flight time came to just over 3 hours for each site, for a total of 6 hours of flight time for just over 2km of river channel and floodplain. This is a great improvement over manual surveys that may normally take more than triple that time to cover the same spatial extent.

### **Structure-from-Motion Image Processing**

To produce orthophotos from the JPEGs images collected during the drone flights, I utilized a commercial-grade structure-from-motion software: Agisoft PhotoScan (now Agisoft Metashape) Professional v.1.4.3. This software uses edge detection and convergent geometries to construct spatial 3-dimensional data from overlapping images. After collecting images, I first inspected the images and removed any that were irrelevant or particularly blurry to avoid contaminating the model. I then used the 'Estimate Image Quality' tool to quantitatively gauge the quality of the remaining images, removing any image that scored below a 0.6/1 in Agisoft's image quality estimation tool. I then aligned the photos, manually removed photos that the software failed to align. This resulted in 200-400 images per orthophoto in both RGB and NIR depending on the study site. I then selected and removed the points with the highest reconstruction uncertainty within the sparse 3-d cloud. The trimmed sparse cloud was then used to generate a dense point cloud



and mesh. The final result is an orthophoto of each site with spatial resolution detailed in Table 5.

Because of the extensive overlap present among raw aerial images (Figure 8), processing time for each orthophoto was increased significantly. The additional overlap was necessary in this flight because of its focus on vegetation, which has been shown to be particularly problematic in SfM applications (Dietrich, 2013). However, even with overlap as extensive as 9+ images for a given point, gaps still occur in the near infrared orthophoto due to the cameras' different FOVs (Figure 9). Future studies should take care to account for the differences in spatial extents of two cameras, perhaps by slightly reducing the photo interval of the drone camera and increasing that of the Canon.

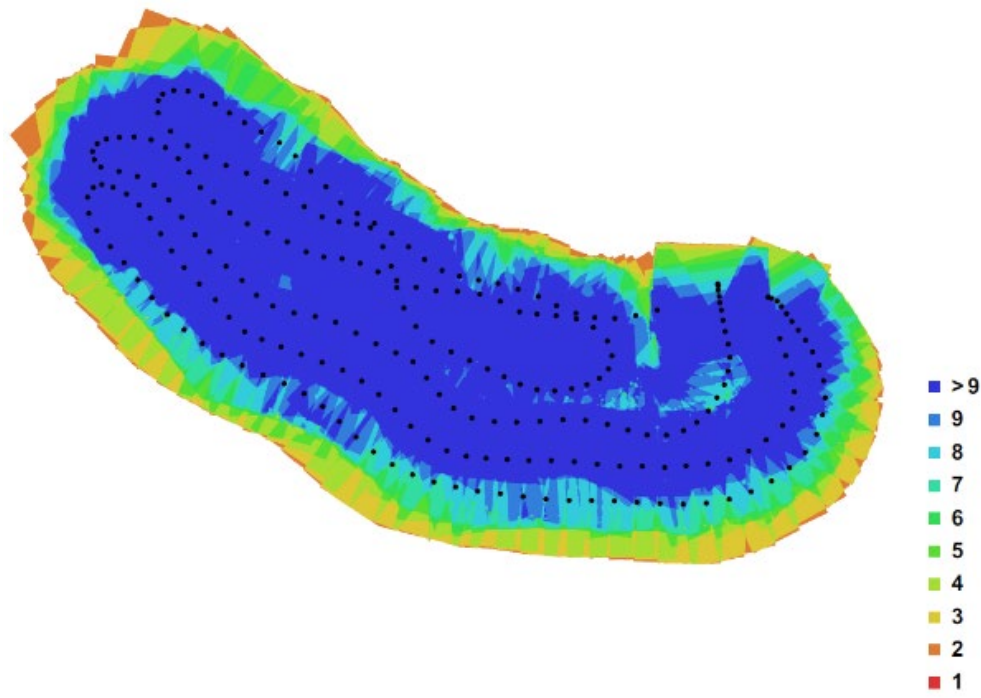
The orthophotos produced by the Phantom 3 JPEGs have an absolute spatial accuracy only as precise as the error present in the drone's onboard GPS. The Canon has no such GPS capabilities – both orthophotos require rectification in order to confidently map change through time. To facilitate rapid imaging of the channel and floodplain, this study utilizes pseudo-invariant orthorectification (see Galiatsatos et al., 2007) that capitalizes on immobile features near the channel throughout each study site, rather than extensive and time-consuming ground control. The drone records spatial data in the WGS-84 coordinate system. I first projected each RGB raster into NAD-83 UTM zone 11 to match imagery flown of each study site in 2013 (see Dietrich 2013). To orthorectify the imagery, 7 points that were located near the channel and were easily identifiable in multiple years of imagery were used to rectify the RGB image (Figure 9). I then georectified each NIR image to its respective RGB orthophoto, assigning them the same spatial reference system. The 4-band stack was then georeferenced to 2013 imagery using

the 7 ground control points in Figure 9 to minimize positional errors and allow comparison between years. Using a spatially uniform equation utilized by (Hughes et al., 2006), the root-mean-square-error between the 2013 and 2018 datasets was calculated to be just under 12cm using the equation:

$$RMSE = [(x_s - x_r)^2 + (y_s - y_r)^2]^{1/2}$$

where  $x_s$  and  $y_s$  are geospatial coordinates of the point on the source image; and  $x_r$  and  $y_r$  are coordinates of the same point on the transformed aerial photo. The RMSE for the whole image is the sum of the RMSE for each coordinate divided by the square root of the number of coordinate pairs. We can thus be confident that any planimetric change detected that is greater than 12cm can be recorded as actual change, while anything below that is within the range of error for the orthophotos.

The use of two consumer grade cameras to create 4-band imagery represents a new and cost-effective method to collect spectral data with the high temporal and spatial resolution facilitated by drones. While most multispectral studies are limited by publicly available satellite images or by the costs of 4-band imaging, this study provides a cheap alternative for practitioners seeking to gain data about vegetation vigor within restoration sites.



200 m

**Figure 8:** Final RGB orthophoto generated for Oxbow Conservation area (top), showing amount of image overlap throughout the study area (bottom). Each dot represents the position of the drone at the time of image capture.

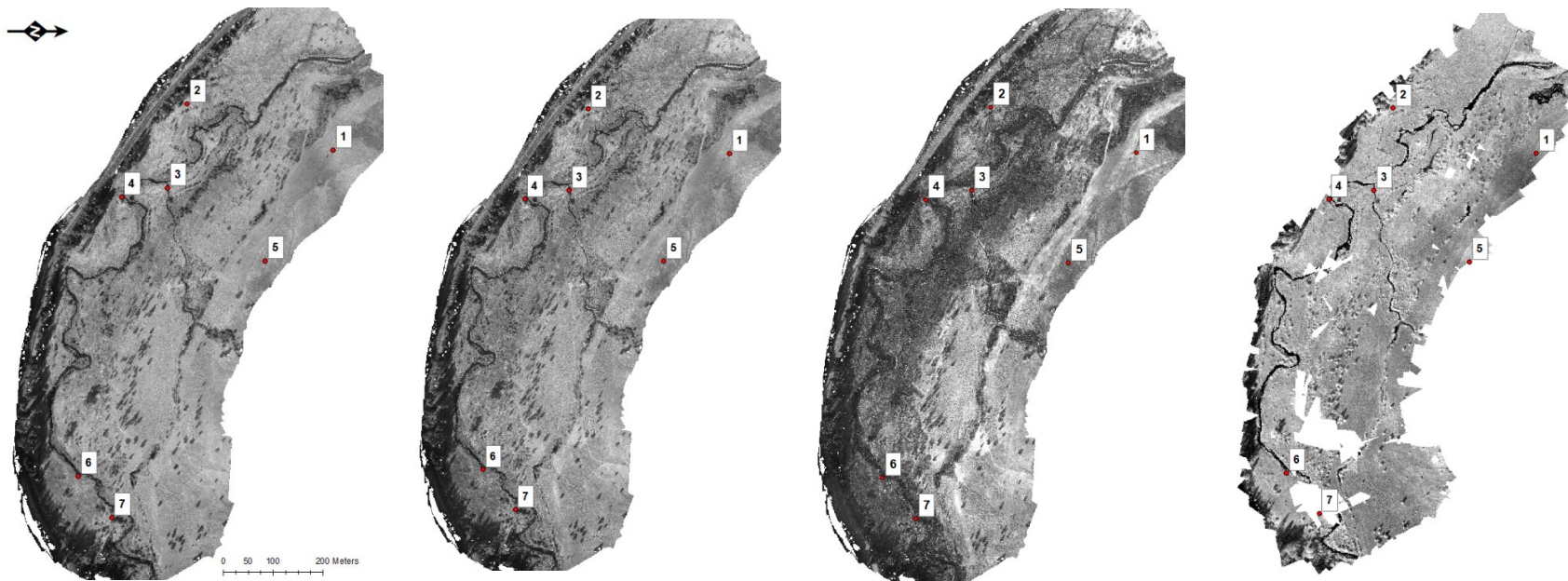


**Figure 9:** Orthophotographs of each band (from left to right: Blue, Green, Red, Near-Infrared) showing ground control points used for georectifying 2018 imagery to 2013 imagery. The gaps in the NIR orthophoto are the result of insufficient overlap in those areas and is partially due to the smaller FOV of the Canon camera in relation to the drone's FC300X.

## CHAPTER IV

### GIS ANALYSIS

Once imagery was collected in the field and orthorectified using SfM, I then implemented a number of GIS analyses to gauge channel and floodplain response to restoration actions. Each technique is described below and summarized in Table 6.

#### **Greenline Digitization**

The greenline is defined as the first line of perennial vegetation that forms a lineal grouping of community types at or near the water's edge (Winward, 2000). A greenline provides an effective way to gauge the establishment of plants along edges of streams. Plant growth at the stream margin is geomorphically significant because of its ability to stabilize streambanks and facilitate meandering morphology in river channels (Perucca et al., 2007, Beechie et al., 2010). To locate the greenline in the field, a line is drawn perpendicular to the channel's centerline, until it intersects with the first continuous line of perennial plants, which can then be sampled to make various conclusions about community change through time. The greenline often corresponds roughly with a channel's planform bankfull width, though this is not always the case (see Figure 10 for examples). The greenline can be easily replicated in a GIS, wherein a polyline is drawn to approximate the location of perennial vegetation stems for each bank. Riparian areas with abundant vegetation near the channel, or growing between the low flow and bankfull water surfaces, may have a greenline to greenline width narrower than bankfull. An incised channel whose floodplain has transitioned to xeric species communities may, in contrast, have a greenline several meters wider than bankfull. The greenline tends to

coincide with areas of high shear stress at the channel margin, which is where one should expect changes to occur more rapidly when examining planform characteristics through time. This makes it a useful feature to study with interannual imagery, especially when vegetation recolonization is a management priority.



**Figure 10:** Greenline location examples under bankfull conditions (left), low flow conditions (center), and areas of erosion and/or incision (right). Note the inclusion of xeric vegetation in the cut bank greenline in the third image. (Source: Winward, 2000)

Because it only samples perennial vegetation that is expected to be stable throughout the year, greenline sampling provides a useful metric that is more or less independent of channel discharge fluctuations and changes in water's edge. The composition of the greenline can serve as an effective proxy for hydrologic connectivity – an abundance of robust hydrophytic plants (e.g., *Carex* and *Salix*) indicates reliable moisture content for at least most of the growing season. Using a vegetation-based metric is particularly appropriate in the context of SfM-derived imagery, which cannot penetrate vegetation for bare-earth applications.

For this study, I digitized three sets of greenlines within a 1.5km section of the MFJD within Oxbow Conservation Area using submeter imagery from 2006, 2013, and 2018. Each greenline was digitized at a scale of 1:125 with a minimum vertex spacing of 1m – any features below this size were not recorded. To track changes in the greenline through time, I generated transects perpendicular to the channel centerline at 2m spacing for the entire study area, recording the distance along the line where the transect

encountered the greenline for each year. To be able to compare the greenline locations through time, I only used a centerline digitized from 2013 to generate the transect locations and azimuths for each year. Changes below the root mean error squared threshold (RMSE) of 12cm were considered to be below the threshold of change detection and discarded. If greenline to greenline width decreased throughout the study period, vegetation should be encroaching on the channel. An increase in greenline-to-greenline width indicates either channel widening or loss of vegetation.

Figure 11 shows an example of the greenline digitized for the same location in two different years – while vegetation is present at the water’s edge in 2013, it does not achieve >60% coverage of continuous perennial vegetation, which pushes the greenline farther from the channel. Figure 12 shows all three digitized greenlines for each bank, with their associated transects generated from the 2013 centerline. With removal of grazing and the restoration of vigorous riparian vegetation, we would expect the distance between greenlines to decrease gradually by year. Results of analysis and subsequent discussion are presented in Chapters V and VI.



**Figure 11:** Greenline location in 2013 (left) and 2018 (right). While some mixed annual/perennial vegetation is present at the water’s edge in 2013, it is not until 2018 that coverage is continuous enough to place the greenline in that location. Flow is from right to left.

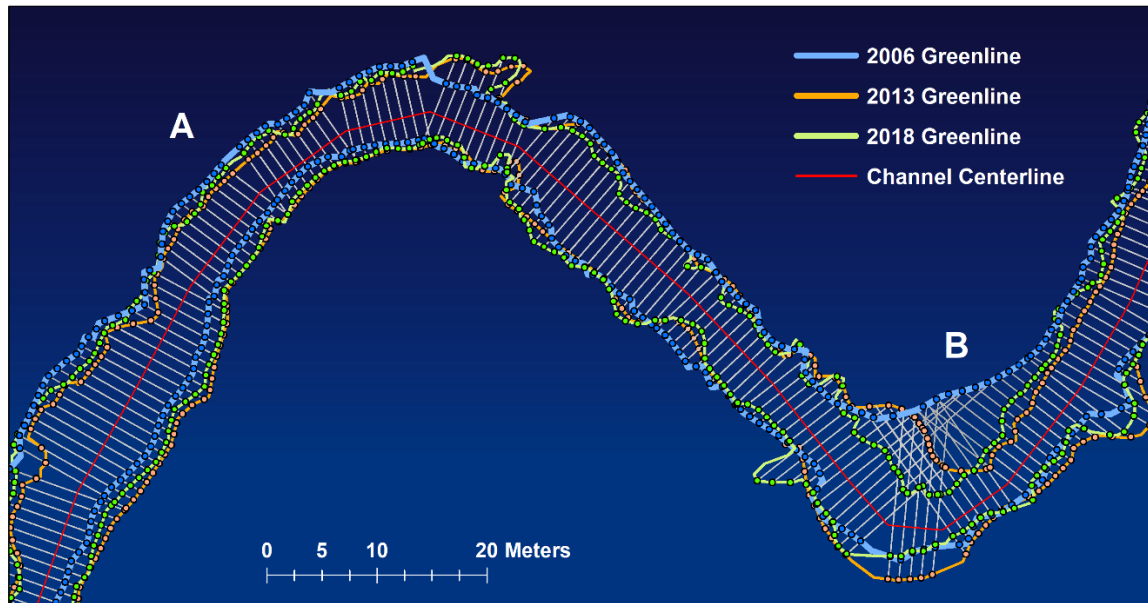


**Figure 12:** Example of fully digitized greenlines showing transects and points of intersection for each year's greenline. At point A, there has been minimal change in the location of the greenline in the 12-year study period. Point B, by contrast, captures perennial vegetation encroachment of nearly 10 meters. Flow in this figure is from right to left. Crossed transects like those present at point B were discarded prior to analysis.

## Vegetation Classification

Maximum likelihood supervised classification is a common tool used in remote sensing to track changes in land cover through time (Strahler, 1980). Within Oxbow Conservation Area and Forrest Conservation Area, little to no woody riparian vegetation existed prior to grazing control and replanting. To gauge the relative abundance of woody and herbaceous vegetation through time within the restored reaches, I divided the RGB imagery into 6 classes based on the apparent moisture content, height, and spectral and textural characteristics of vegetation patches. Further subdivision tended to result in misclassification due to similar spectral properties. While it lacks the species-level



precision of field-based data collection, classification and change detection can be a powerful tool to estimate change through time in relative abundance of functional plant groups. GIS classification helps to estimate canopy cover, tracking closely with restoration goals of increasing stream shade and reducing solar loading on the channel. It is important to track vegetation composition and height through time in order to identify problem areas or places to be maintained. Additionally, imagery-based classification can supplement quantitative vegetation sampling in the field which may not be feasible to do every growing season.

To create training classes to identify vegetation groups, I used orthorectified submeter resolution RGB imagery stacked with a DEM for 2006 and for 2018. The 2006 DEM was sourced from highest-hit lidar data, and the 2018 DEM was sourced from SfM processing. Both effectively sample the vegetation height and return those values in a raster format and so are roughly comparable to each other. Figure 13 gives an example of classified imagery.



**Figure 13:** Example of classified imagery in Oxbow Conservation Area. The classification performs best for differentiating dry and wet herbaceous material, water, and large woody debris.

The efficacy of classification was variable depending on the class itself and is discussed in detail in Chapter V.

To track changes in near-channel and floodplain landcover through the 12-year study period, I generated a change matrix for all landcover classes between 2006 and 2018, using the pixel counts of each landcover class to assess relative abundance within the study area. The 2006 imagery and the 2018 imagery were collected during late summer / early fall conditions and are more comparable in terms of their late summer soil moisture and vegetation composition. 2013 and 2018 were not compared because the floodplain in 2013 contained abundant vigorous seasonal herbaceous vegetation that would bias the results towards showing more recovery than is strictly due to restoration and replanting efforts. I therefore only compared 2006 and 2018 to control for the seasonal differences in vegetation.

### **NDVI Analysis**

The Normalized Difference Vegetation Index, or NDVI, is one of the most commonly used indices in vegetation remote sensing, and is generated using the equation developed by CJ Tucker (1979):

$$NDVI = \frac{\rho_{nir} - \rho_{red}}{\rho_{nir} + \rho_{red}}$$

where  $\rho_{nir}$  represents reflectance in the near infrared band and  $\rho_{red}$  is reflectance in the red band. Indices are useful to remove the effects of shadows, which aids in the classification and interpretation of imagery. The NDVI takes advantage of the fact that healthy plants are relatively dark in the visible red portion of the electromagnetic spectrum and relatively bright in the near-infrared. Examining this in map form can yield

valuable information about the spatial distribution of vigor, and subsequently help identify areas of particularly vigorous or stressed vegetation (e.g., Zhou et al., 2001). This study utilizes the multispectral imaging system described in Chapter III to gain a rough estimate of vegetation vigor within Oxbow CA and Forrest CA.

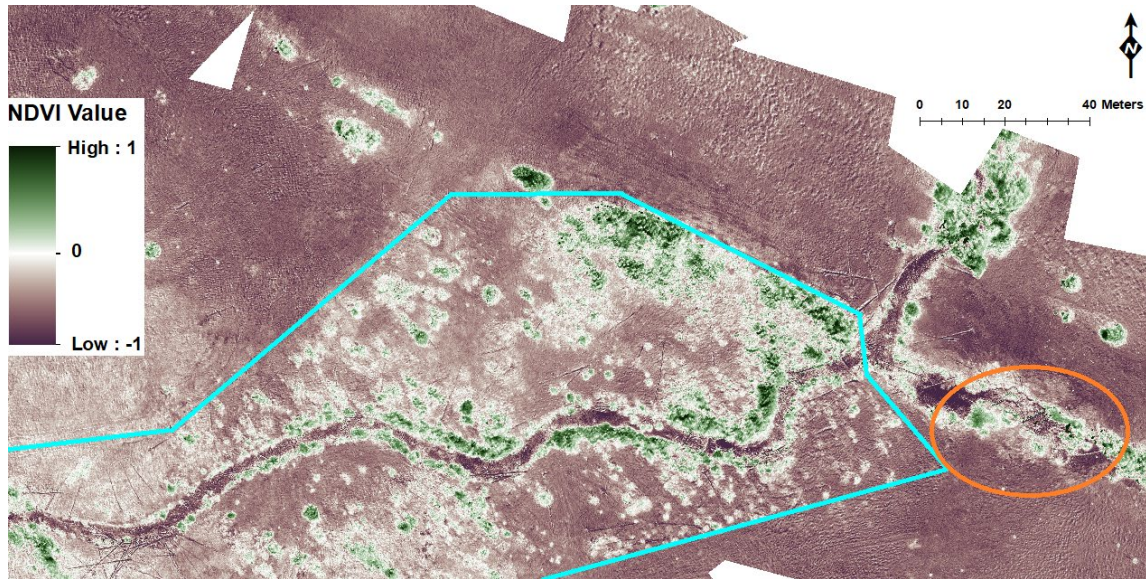


**Figure 14:** Subset of NDVI imagery focusing on restored portion of Granite Boulder Creek. Dark areas show the low values associated with water and mine tailings. Plantings near the channel have the highest NDVI values, while hardwood trees planted farther away are in early fall senescence with accordingly lower values. The fence bordering the restored riparian area of Granite Boulder Creek is outlined in blue, and the alcove formed by a remnant portion of the decommissioned north channel is circled in orange.

I used calibrated red and near infrared orthophotos to produce NDVI maps. Because the 2018 imagery was flown during mid-September, the signal resulting from seasonal precipitation should be at its weakest, and vegetation vigor should correlate with areas of hydrologically connected floodplain with more available groundwater. I then interpreted the NDVI values to assess areas of relatively vigorous vegetation and areas of potential concern, with an emphasis on replanted areas. A portion of the restored floodplain of Granite Boulder Creek is shown below in Figure 14 and shows the area

fenced in to reduce browse pressure. Dark values indicate mine tailings or bare earth. The higher NDVI values near the alcove on the right side of the image are remnants of former streamside vegetation on the decommissioned north channel in Oxbow CA.

### **Large Woody Debris Assessment**

Much of the active restoration that has been implemented in the MFJD has a significant emphasis on reintroducing large woody debris to the channel. Large woody debris (LWD) is a well-known and important physical component of in-channel habitat for a range of aquatic species – particularly juvenile salmonids – and is thus important to monitor in restoration contexts through time. Within Oxbow Conservation Area, LWD structures were designed primarily to facilitate bank stabilization while allowing for the maintenance of deep pools by promoting scour (see Abbe & Montgomery, 1999). LWD structures at this site were intended to be stable through time while maintaining scour pools built during active restoration. Rapid visual assessment in imagery provides a straightforward and intuitive way to gauge each structure's behavior through time, and track how many pieces are being lost or recruited within a given structure. Additionally, a human eye is more adept at noticing wood pieces that may be submerged, and thus not readily accounted for in the classification scheme in part ii of this study's analysis.

To analyze the LWD structures within Oxbow, I used all three submeter resolution RGB orthophotos separated into 50m zones based on distance downstream on the channel centerline (although it has been used in past multispectral studies of LWD, near infrared information was not necessary at the submeter resolution). I then recorded the number of large wood pieces over 7m in length and with a diameter >0.2m per 50m segment of

channel to approximate the minimum size requirements for LWD as defined in the USFS stream survey handbook for Pacific Northwest rivers east of the High Cascades (USFS, 2012). LWD outside the active channel margin was not tallied. I then produced a longitudinal count of wood abundance per unit for 2006 (pre-restoration), 2013, and 2018. For several structures that had seen change between the 2013 and 2018 flights, a simple comparison of the same location in two years often revealed which pieces of LWD had moved downstream.

**Table 6 | Summary of Raw Data Formats and Analysis**

<i>Site Feature</i>	<i>Raw Data</i>	<i>Analysis</i>	<i>Monitoring Application</i>
Planform Channel Change	RGB imagery from 2006, 2013, 2018	Greenline migration rate from 2006 – 2013, and 2013 – 2018. Visual identification of change hotspots	Large woody debris and channel greenline margins digitized from imagery in ArcGIS. Migration and LWD stability assessed through a 12-year period utilizing 3 sets of high resolution imagery.
Riparian Zone Composition	2018 greenline survey data, 2018 floodplain polygons & 2014, 2018 drone imagery	Supervised classification using spectral and textural properties of vegetation communities	Vegetation classes compared with 2018 floodplain mapping, visual assessment to determine the extent of riparian community change.
Riparian Zone Vigor	RGB + NIR Imagery	Analysis of normalized difference vegetation index (NDVI)	NDVI images used to assess relative levels of vegetation vigor throughout the study site – higher levels of NDVI correlated with higher late-summer soil moisture and floodplain connectivity.

## CHAPTER V

### RESULTS

#### **Greenline**

The distance between the 2013 channel centerline and the 2018 greenline has generally decreased within Oxbow Conservation Area. Figure 15 shows that the distance between left- and right-bank greenline has generally decreased throughout Oxbow Conservation Area. The values summarized in figure 15 were generated by subtracting the distance from the 2013 centerline-greenline distance from the 2018 distance along the same transect. A negative value shows that the 2018 width was smaller than 2013, indicating narrowing of the greenline. The data are roughly normally distributed with a mode near zero and a slight negative skew, indicating that vegetation has, on average, encroached on the channel by 0.89 meters between 2006 and 2018. It is notable that there far more areas of distinct vegetation encroachment than retreat. Areas of encroachment primarily occur inside meander bends (Figure 16), where areas of gravel bars that were exposed in 2006 that have been rapidly recolonized by riparian vegetation. The greenline additionally tracks well with active channel processes, and captures bank erosion downstream of several large wood structures. The most dramatic change in the greenline occurred between 2006 and 2013, most likely as a result of grazing removal in 2002. The signal captured is primarily due the encroachment of *Salix* and *Carex* species. Woody plantings that do not overhang the channel are not captured by the greenline, but should be increasingly represented through time as canopies become larger and begin to gradually intersect the bank.

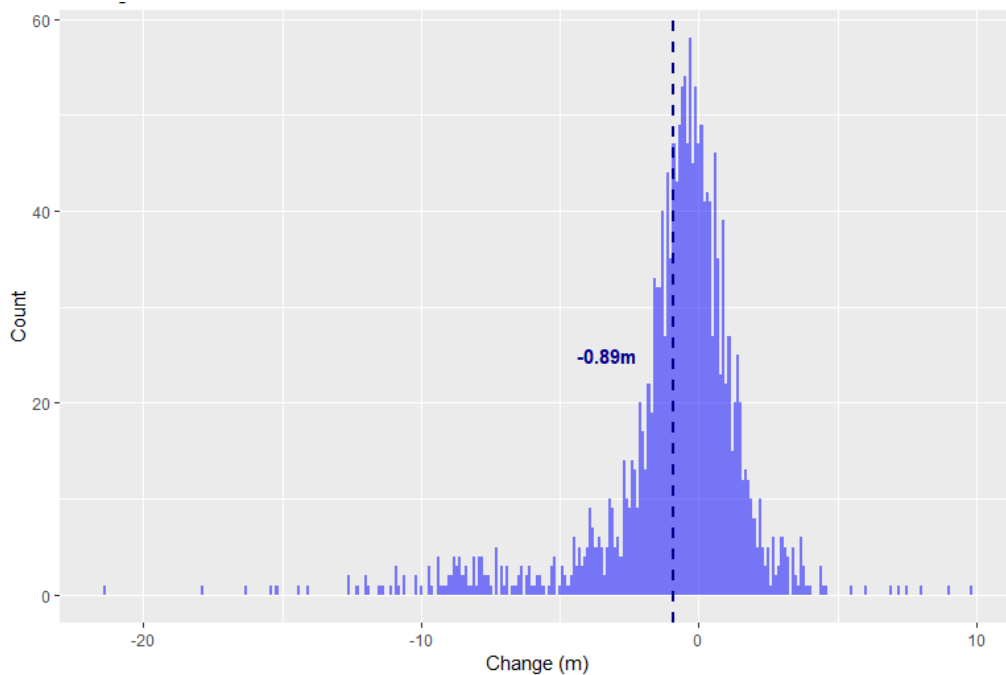


**Figure 15:** Change in greenline to greenline width, 2006 – 2018. The average throughout the study site is indicated by the dark dashed line

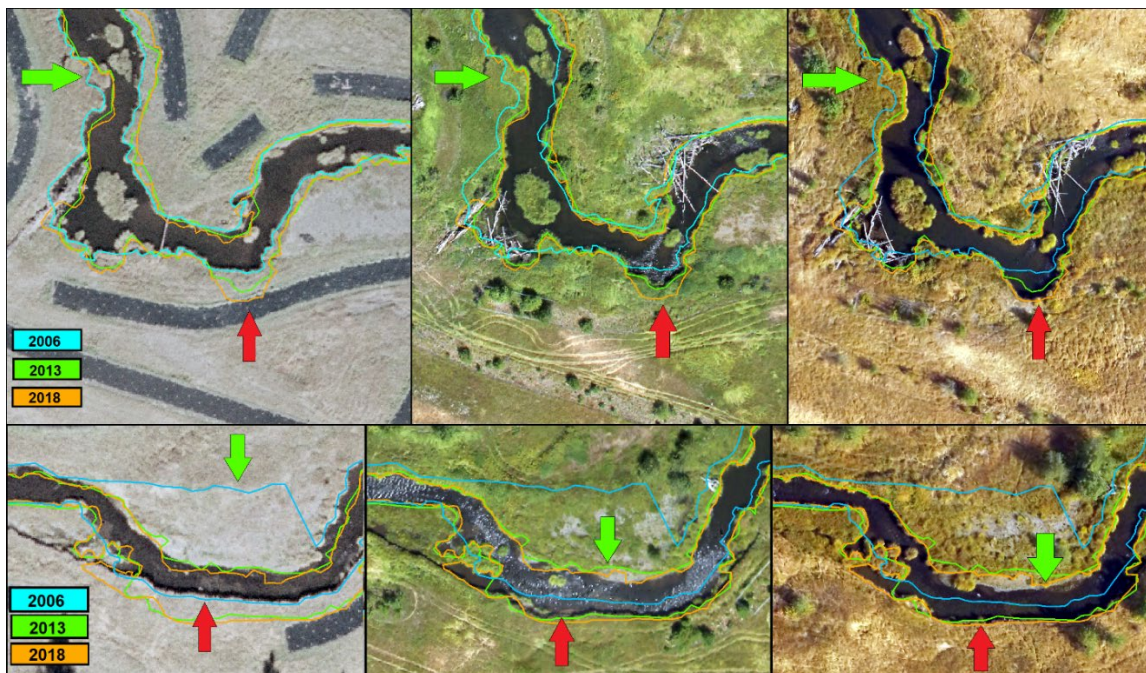


**Figure 16:** Hotspots of greenline change showing all three greenlines across 2006 imagery (left), 2013 imagery (center), and 2018 imagery (right). Red arrows indicate areas of erosion or retreat. Green arrows highlight areas where vegetation has encroached on the channel.



Figure 17 shows the greenline migration for each bank. Of the change visible between 2006 and 2018, the vast majority occurred between 2006 and 2013. Separating migration into right and left banks (facing downstream) additionally reveals that the right bank shows considerably more change than the left bank. Throughout the study period, the left bank was far less mobile than the right, with a total mean change below the RMSE of 12cm. Interestingly, when separated into two time periods, the right bank first widens by 0.3m between 2006 and 2013, and narrows by 0.25 from 2013 to 2018. By contrast, the right bank's greenline moved closer to the centerline throughout the study period, and is the primary cause of the average narrowing in Figure 15.

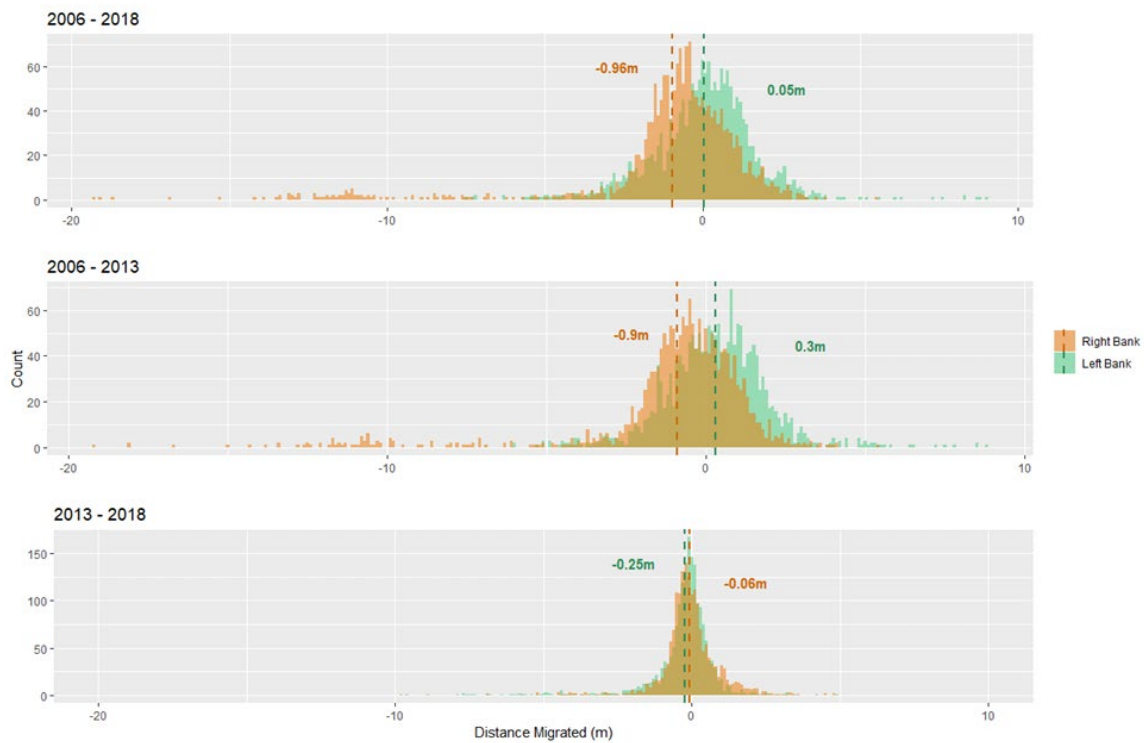


**Figure 17:** Change in distance from greenline to channel centerline separated into left bank (green) and right bank (orange) organized by time interval. The top histogram includes the entire study period, while the second two are broken into two consecutive time intervals. Negative values show movement towards the channel centerline, while positive values indicate greenline movement away from the centerline. The numbers in bold indicate mean change for each bank.

## Landcover Composition

A summary of landcover composition change is provided in Table 7, and the pixels counts used to generate them can be found in Table 8. Between 2006 and 2018, there was an increase in bare earth, large woody debris, dry herbaceous vegetation, and wet herbaceous vegetation. Open water and woody vegetation decreased slightly, and black plastic tarps were no longer visible in 2018. The decrease in water and woody vegetation is primarily due to the decommissioning of the north channel, where landcover has mostly changed to either herbaceous vegetation or reverted to bare earth. Although the overall pixel count of woody vegetation decreased, woody vegetation in 2018 is much less intermixed with bare earth and dry herbaceous vegetation, indicating that woody riparian plants are filling in and becoming more established.

Supervised classification in RGB was effective in this study site largely due to the patchiness of vegetation. Long shadows from nearby ponderosa pines were frequently miscategorized as water. The classification did surprisingly well with large woody debris, with the exception of some misidentification of bright bare earth. Because riparian vegetation is particularly prone to mixed pixels even at submeter resolutions, only three classes of vegetation were used.

**Table 7 | Percent Composition of Land Cover Classes by Year**

Landcover Class	2006	2018	% Change
Bare Earth	24.9%	31.2%	+ <b>25.6%</b>
LWD	0.04%	0.5%	+ <b>1,101.2%</b>
Dry Herbaceous	35.1%	32.2%	+ <b>8.0%</b>
Wet Herbaceous	24.1%	26.6%	+ <b>10.1%</b>
Woody Vegetation	7.8%	6.5%	- <b>17.0%</b>
Black Plastic	2.8%	0	- <b>100.0%</b>
Water	5.2%	2.9%	- <b>44.2%</b>

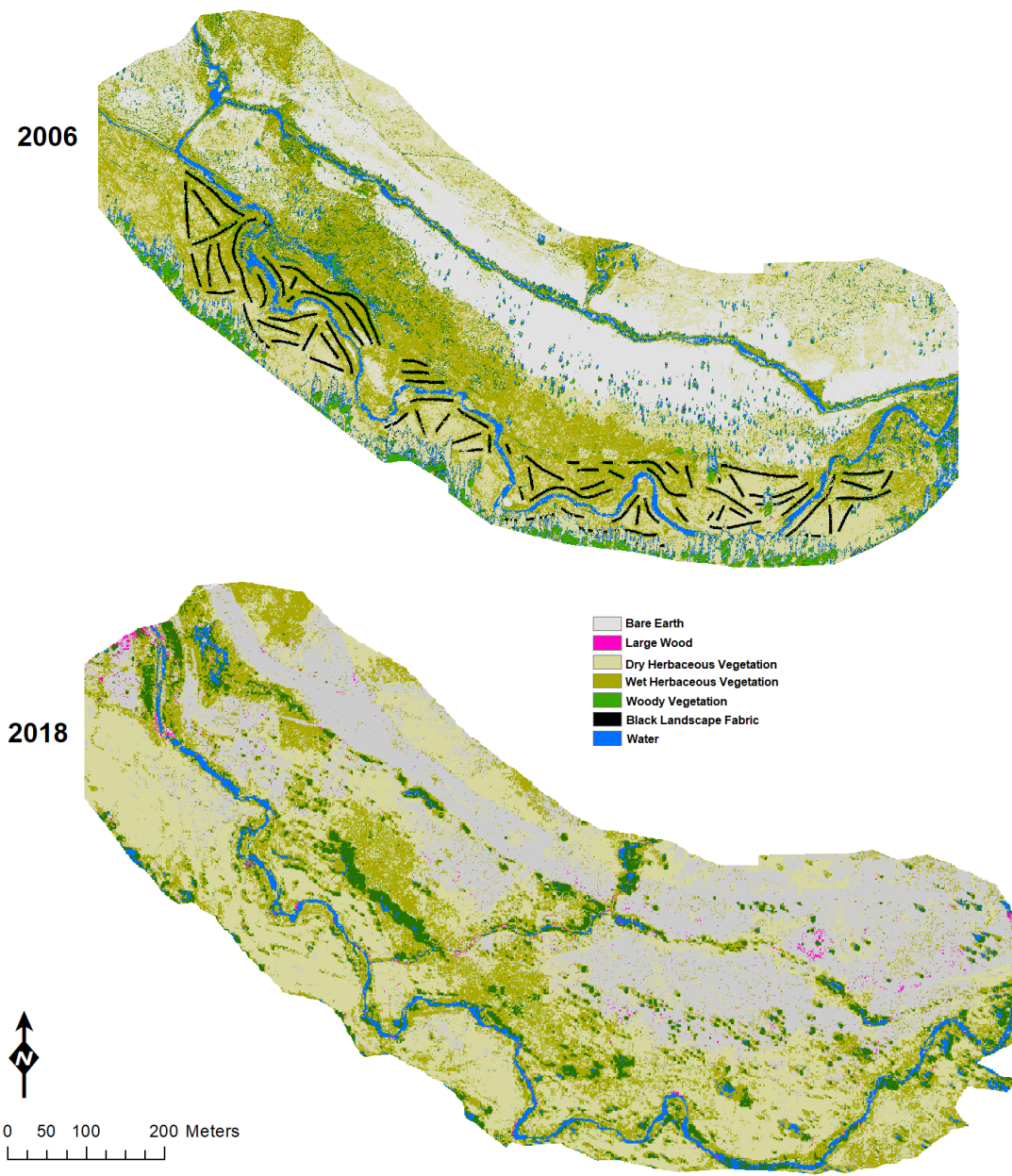


**Figure 18:** Map results of supervised classification within Oxbow Conservation Area

**Table 8 | Change Matrix of Classified Pixels at Oxbow CA**

Pixel Class	Bare Earth	LWD	Dry Herbaceous Vegetation	Wet Herbaceous Vegetation	Woody Vegetation	Black Plastic	Water	Sum (2006)
Bare Earth	<b>67574.7675</b>	866.34	19280.565	11821.2075	2690.91	0	546.165	102779.955
LWD	57.6675	<b>1.7775</b>	43.695	50.715	15.255	0	9.1125	178.2225
Dry Herbaceous Vegetation	42735.9375	587.1825	<b>57953.655</b>	34525.0575	6125.49	0	2839.095	144766.4175
Wet Herbaceous Vegetation	9364.6575	228.645	40175.4825	<b>40766.6025</b>	7602.075	0	1596.6225	99734.085
Woody Vegetation	5636.0025	183.87	7776.5625	11870.415	<b>5450.6925</b>	0	1414.6425	32332.185
Black Plastic	1237.3875	15.705	4774.0725	4097.9025	1300.7475	<b>0</b>	234.54	11660.355
Water	2438.64	257.2425	3144.2175	6658.7175	3658.1625	0	<b>5370.975</b>	21527.955
Sum (2018)	129045.06	2140.7625	133148.25	109790.6175	26843.3325	0	12011.1525	<b>412979.175</b>

## Vegetation Vigor

NDVI values calculated for Oxbow Conservation Area are summarized in Figure 19 and mapped in Figure 20. Because there are no calibrated measurements of NDVI prior to this imagery, these images can serve only as a point in time descriptions of vegetation vigor within the site and cannot indicate change without multitemporal imaging. The lowest NDVI values within both study sites correspond with areas of bare earth – at Oxbow, this primarily reflects the dredge tailings near the decommissioned north channel. The highest values correspond with near-channel *Alnus* and *Salix* clusters, as well as stands of *Pinus ponderosa* on the hillslopes near the southern extent of the site.

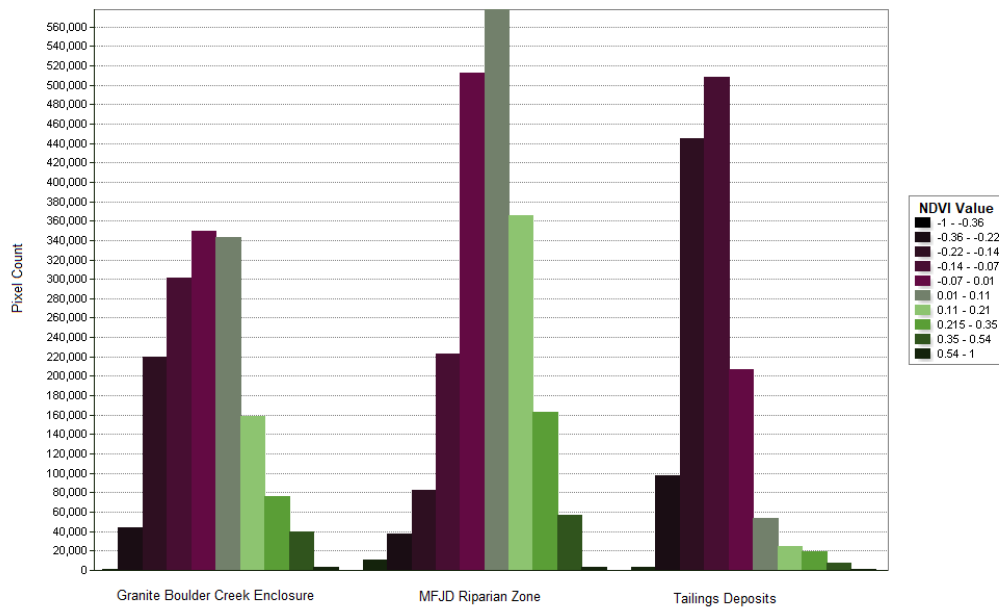


**Figure 19:** Histograms of NDVI values for contrasting areas of Oxbow CA

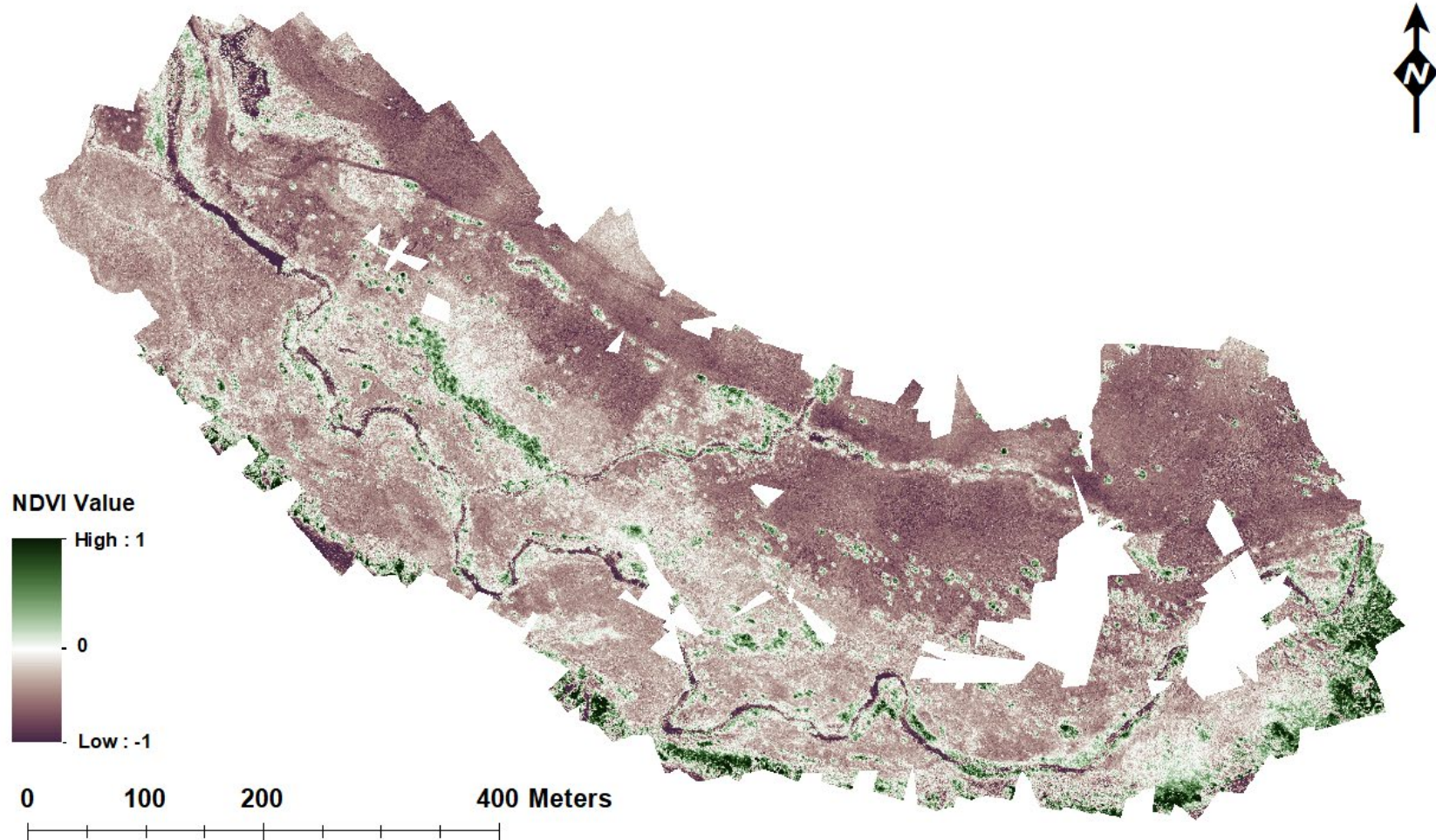


**Figure 20:** NDVI Map of Oxbow Conservation Area  
Spatial Resolution: 4.3cm/px

Most of the riparian zone within Oxbow CA has an NDVI value between 0.1 and 0.3, which is consistent with late summer conditions and drought stress in semi-arid floodplains. Remnant vegetation along the decommissioned north channel maintains a value similar to the riparian zone of the south channel, and the plantings within the restored portion of Granite Boulder Creek near the center of the map show notably higher values than the bare earth outside of the deer and elk browse exclosures (Figure 14, Chapter III shows a subset focusing on Granite Boulder Creek). Mid-channel *Carex nudata* islands are visible within the mainstem MFJD and maintain values between 0.2 and 0.3. Plantings within exclosures around old planting strips, particularly in the southwestern portion of the map, maintain some of the highest near-channel NDVI.

Imagery with 1.5cm resolution taken at Forrest Conservation reveals variations at the scale of individual plants. Figure 21 shows a fenced area of plantings adjacent to the MFJD containing 6 planted trees. The highest NDVI values are near the center of the exclosure. The shrub near the water's edge near the top left of Figure 21 is an alder that has not been protected from browse, which may partially explain its lower NDVI values. These values, while fundamentally descriptive and observational in nature, help to paint a clearer picture of the success of riparian revegetation success within the study areas.

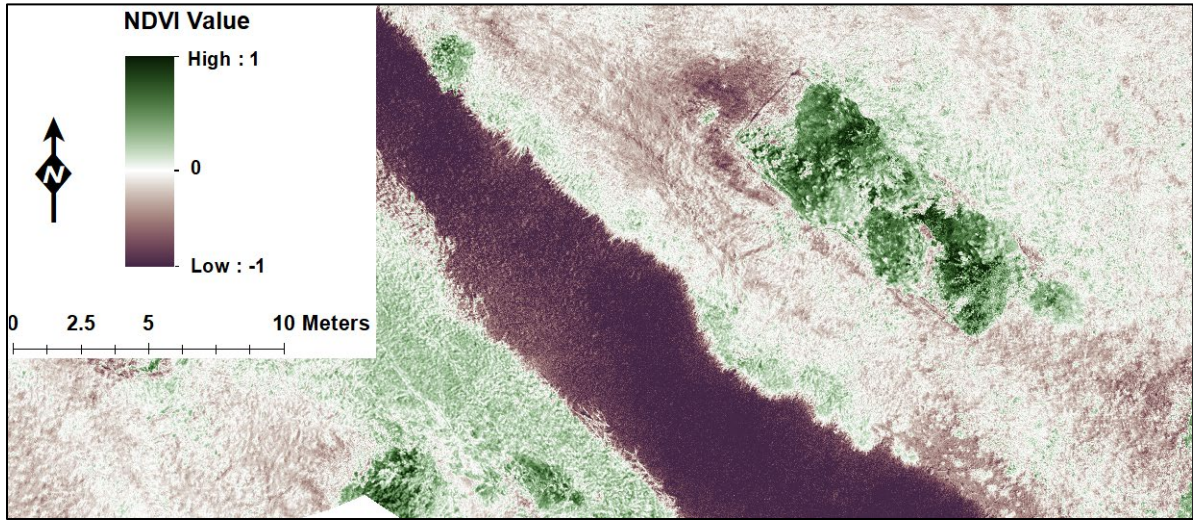


**Figure 21:** Subset of Forrester NDVI map, showing values at the individual plant scale  
Spatial Resolution: 1.5cm/px

### **Large Woody Debris Assessment**

In 2006, there was virtually no large wood with a length >7m in the mainstem MFJD, for a total count of 6 pieces. In 2013, active construction of LWD structures made for a total count of 104 pieces – this total remained the same in 2018. Results from analysis of 2013 and 2018 imagery show that large wood within Oxbow Conservation is mostly stable. Figure 22 shows the downstream abundance of large wood plotted by 50m unit for each year of aerial imagery. Between 2013 and 2018, abundance has remained constant, but the distribution within Oxbow has become somewhat less clustered, with some downstream movement of wood (see Figure 23 for examples).





**Figure 22:** Downstream abundance of LWD organized by year

The vast majority of wood structures within the study site have remained stable, keeping in line with the goals of restoration design. Loose pieces within the study reach have undergone some redistributing and downstream movement. Figure 23 gives visual examples of wood movement within Oxbow CA. The first pair of images shows downstream movement of roughly 50 meters that remains within the same unit. The second image pair shows the movement of 2 loose pieces downstream into two different units. The bottom pair of images shows a stable logjam accumulating loose wood from upstream.

2013

2018

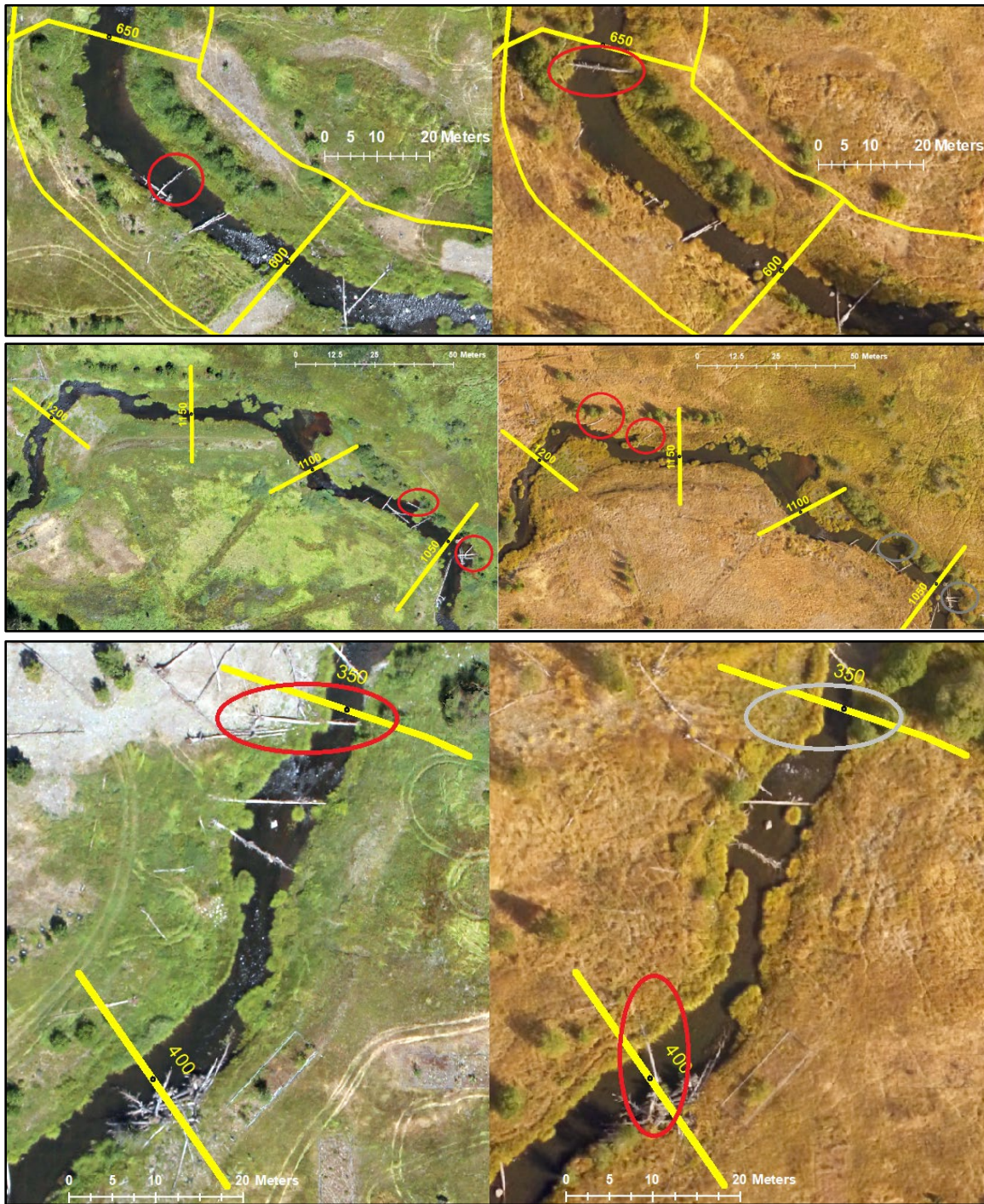


**Figure 23:** Examples of wood movement within the study area for June 2013 (left), and September 2018 (right). The yellow lines indicate distance downstream in meters from the beginning of the study site, and were used for unit breaks to bin LWD. Red circles show individual pieces of wood identifiable in both years of imagery.

Reorganization of large wood is summarized in Figure 24, which shows the addition or removal of pieces from individual bins between 2013 and 2018. Note that the upstream-most bin has accumulated wood and the 2 bins farthest downstream have lost wood, indicating that wood has both entered and exited the system. Several large structures towards the upstream extent (distance <500) were only partially reinforced, and should expect some downstream movement of wood pieces. The largest change for any given unit within the study area is 5 pieces of wood.

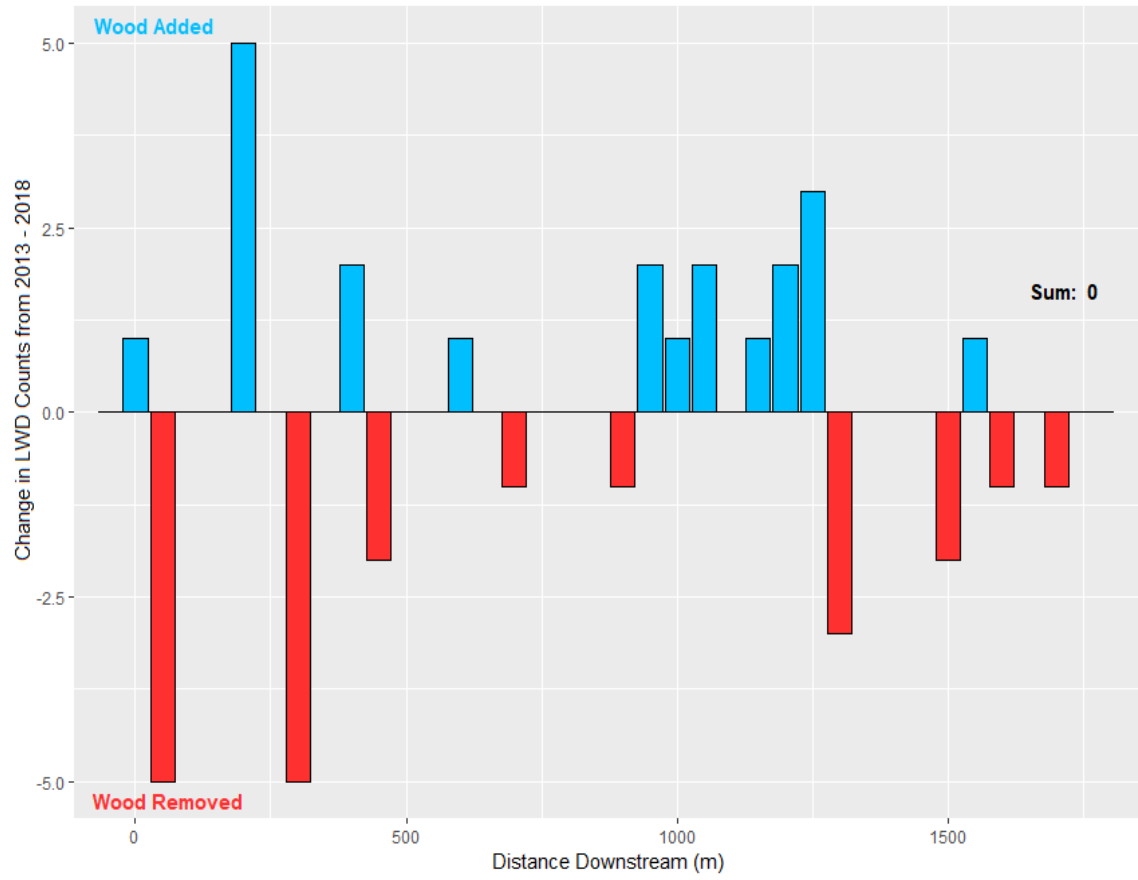


**Figure 24:** Change in LWD distribution between 2013 and 2018.

## CHAPTER VI.

### DISCUSSION OF RESULTS

Results from Chapter V show that the MFJD is generally moving towards long-term restoration goals. Vegetation response is consistent with the expected disturbance and recovery timeline of active restoration, and greenline narrowing shows progress towards restoration goals of increased fish cover and reduced solar loading. Large woody debris has been mostly stable and aligns with restoration goals.

#### **Vegetation and LWD Monitoring**

Between 2006 and 2018, greenline-to-greenline width decreased throughout Oxbow Conservation area, with notable hot spots of narrowing at meander inflection points. The majority of change hotspots coincide with areas of rapid colonization of exposed substrates by *Carex nudata*, which produced the strongest channel narrowing signal within the study period. Cross sectional data gathered in the same study area, by contrast, does not share the same pattern (Middle Fork IMW, 2017) and indicates that narrowing is primarily the result of riparian vegetation encroachment, rather than active channel processes. Naturally recruited, flood-tolerant plant groups including *Carex*, *Salix*, and *Alnus* clusters are the most well represented in the 2018 greenline, while the 2006 greenline primarily samples xeric species farther from the channel centerline. This shift in community composition likely represents the re-establishment of shoreline fringe and bank zone plants in response to cattle grazing removal. Imagery derived greenline analysis is therefore a useful metric for gauging the initial response to grazing removal –

it will not, however, effectively sample near-channel plantings until they have canopies that overhang the channel.

Key pieces of wood are mostly stable within Oxbow Conservation Area, with some reorganization of loose pieces within the study reach. This is mostly in line with intentions of restoration that sought to anchor large wood permanently in the channel margin. Practitioners primarily expect wood structures to create and maintain scour pools that create cold water refugia for salmonids (Middle Fork IMW, 2017). Movement of large wood pieces within the study reach from 2013 to 2018 has been minimal, with no more than 5 pieces lost or gained within a given 50m length of channel. This may in fact aid the further development of LWD-mediated scour pools in areas beyond the original structures, provided that the mobile pieces become stable in time. Visual inspection of individual logjams shows some slight change and adjustment in the angle of key pieces. It is important to note that no significant flooding occurred between 2013 and 2018, so it is possible that much of the change simply may not occur outside stronger floods. More years of surveys will paint a clearer picture of LWD structure performance and redistribution of pieces within the study area.

### **Floodplain Mapping**

Supervised classification illustrates that the overall extent of woody vegetation has decreased slightly –this is primarily a function of disturbance from active restoration, as the infilling of the dredged north channel removed several areas of mature riparian vegetation. While large woody debris is usually considered to be quite difficult to distinguish from bare earth in RGB classification, its classification performed remarkably

well in this study (Figure 26). This is likely a result of the spectral conditions at the time of flying – mixed pixels of dormant grasses and bare earth scattered through the floodplain give them a slight red tint that helped distinguish bright bare earth from large wood.

In addition to this research, mapping done by walking the extent of the MFJD floodplain and digitizing vector community extents by tablet was completed in summer 2018 by Ellsworth et al (2018). This provides an opportunity to compare map results of two methods. Results of 2018 field mapping are shown below in Figure 25. A comparison of the two maps fundamentally reveals the tension between spatial extent and resolution present in any geographic study. Vector floodplain mapping lists the dominant species of a given area of floodplain, with the areas of each polygon determined by the mapper in the field. The vector map provides valuable information about dominant species that is independent of scale. For example, it successfully captures the presence of cheatgrass (*Bromus tectorum*) in the north floodplain and Nebraska sedge (*Carex nebrascensis*) near the channel that are small, non-clumping species outside the realm of feasible identification achievable with drone imagery. This species level identification and mapping is made practically feasible only by generalizing spatial variation across larger areas.

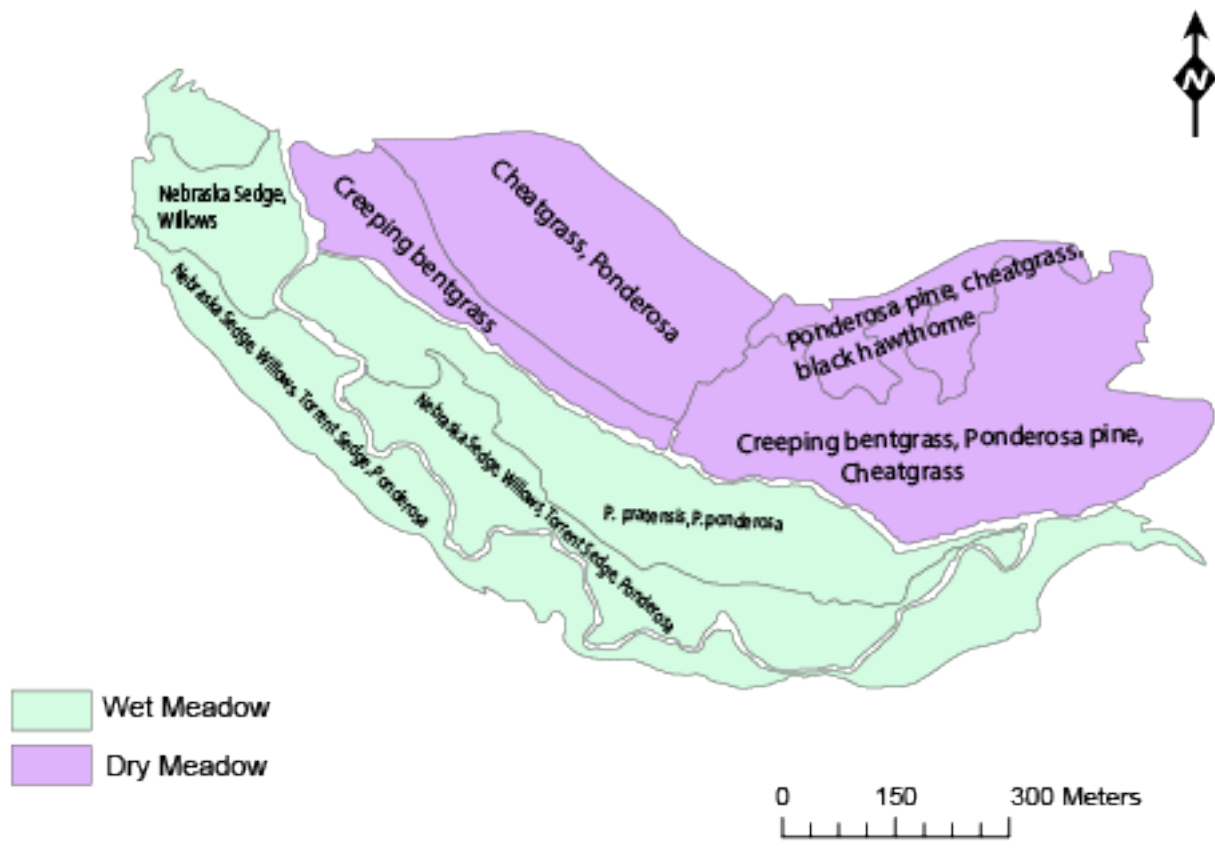
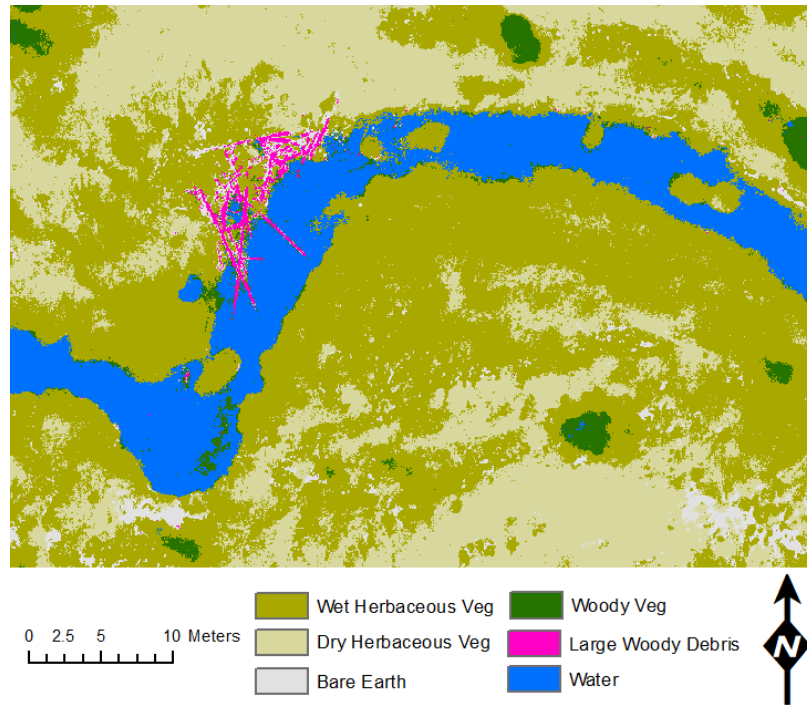


Figure 25: Vector floodplain map generated from field surveys showing dominant species





**Figure 26:** Example of supervised classification outputs from drone imagery

Supervised classification of high-resolution imagery provides fundamentally different information that hints at finer spatial resolution patterns of hydrologic connectivity, consolidation of vegetation clusters and expansion of plantings within enclosed areas. Additionally, the classification showed patterns of near channel vegetation change that were not present in the vector maps. While the vector mapping draws broad difference between wet and dry meadow (Figure 25), classification of dry and wet herbaceous vegetation reveals depressions within the floodplain receiving comparatively more moisture and supporting different communities along a spatial continuum better suited to gauge landscape function. Future work might attempt species level identification from drone-based imagery using extensive ground control and validation to assess its potential.

## **NDVI Performance**

NDVI mapping shows that deer and elk browse exclosures are working well and generally maintain the highest levels of vigor during late summer moisture stress. Some areas of riparian plantings show comparatively low values, but these are correlative with other near-channel vegetation that predates restoration. The effects of shadows, though minimal, were still apparent in NDVI maps. Shadows from large trees show relatively high values towards one side, and darker towards the opposite, and are a likely result of slight inaccuracies in georectifying the red to the near infrared band (see Figure 27). Some speckling was also present – a common side effect of using indices with high resolution imagery. NDVI is thus effective for showing spatial patterns of vegetation health, but no strong conclusions can be made with a single point in time measurement. However, the maps show promise that exclosures are performing well and that reducing browse pressure may help reestablishment of riparian woody vegetation. Future research could re-image enclosed areas to evaluate change in NDVI through time. As vegetation becomes more established and more drought tolerant, it should track with increased late-season NDVI values.

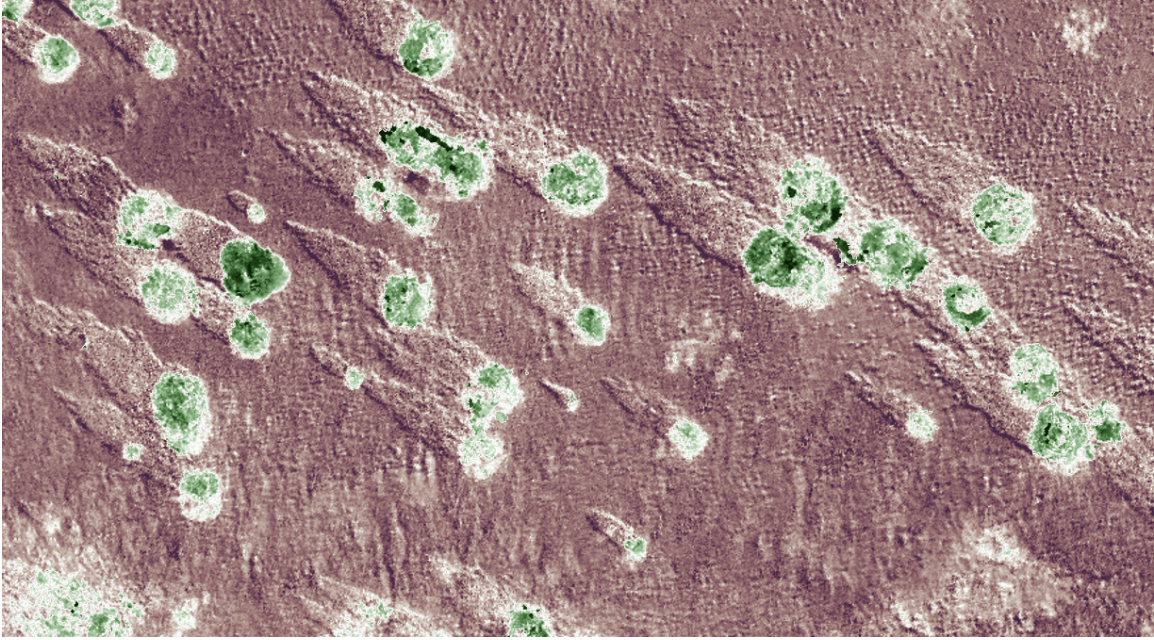


**Figure 27:** Example of shadow effects from tall Ponderosa pine trees in NDVI map. Green areas correspond to individual trees.

## CHAPTER VII.

### CONCLUDING COMMENTS

This research has shown one application of using UAV-derived data to monitor restoration effectiveness quickly and effectively, and presents applications that may be particularly useful to practitioners working in semi-arid streams where loss of riparian vegetation is among the primary causes of habitat impairment. UAV imagery has proven to be a reliable source of spectral data, with useful applications in both visible and near-infrared spectra. This research has also shown how the spectral limitations of consumer grade cameras can be overcome with proper calibration to aid in analysis. Here, the production and calibration of 4-band imagery, as well as the NDVI index, was made possible with the use of a spectrometer and cheaply modified Canon camera, and revealed useful information about the performance of enclosed riparian plantings within the floodplain and, consequently, the impacts of wild ungulate browses. I have also shown that supervised classification can be a useful tool to track changes in land cover through time in a restoration context.

This research was successful in using greenline methodologies developed in the field within a GIS context, and extracting a narrowing signal not present in other geomorphic studies of this reach. NDVI calibration could be greatly improved by the use of more low-reflectance panels, which would fix the under-prediction of reflectance values for water surfaces and sparsely vegetated areas of the floodplain. To advance this research I suggest careful planning of drone flights to ensure proper coverage, as well as

the inclusion of species-specific vegetation ground control to test higher resolution identification for assessing restoration goals.

High quality monitoring data is a critical component of adaptive management. It is important to constantly reassess our methods and principles in order to meet the ecological challenges of the next century. Continued research in methods development for restoration monitoring will help give researchers and practitioners the tools, skills, and understanding necessary to manage landscapes for the greatest possible success and resilience.

## REFERENCES CITED

- Abbe, T. B., & Montgomery, D. R. (2003). Patterns and processes of wood debris accumulation in the Queets river basin, Washington. *Geomorphology*, 51(1–3), 81–107. [https://doi.org/10.1016/S0169-555X\(02\)00326-4](https://doi.org/10.1016/S0169-555X(02)00326-4)
- Beechie, T. J., Sear, D. A., Olden, J. D., Pess, G. R., Buffington, J. M., Moir, H., ... Pollock, M. M. (2010). Process-based Principles for Restoring River Ecosystems. *BioScience*, 60(3). <https://doi.org/10.1525/bio.2010.60.3.7>
- Bennett, S., Pess, G., Bouwes, N., Roni, P., Bilby, R. E., Gallagher, S., ... Greene, C. (2016). Progress and Challenges of Testing the Effectiveness of Stream Restoration in the Pacific Northwest Using Intensively Monitored Watersheds. *Fisheries*, 41(2), 92–103. <https://doi.org/10.1080/03632415.2015.1127805>
- Berra, E. F., Gaulton, R., & Barr, S. (2017). Commercial off-the-shelf digital cameras on unmanned aerial vehicles for multitemporal monitoring of vegetation reflectance and NDVI. *IEEE Transactions on Geoscience and Remote Sensing*, 55(9), 4878–4886.
- Bizzi, S., Demarchi, L., Grabowski, R. C., Weissteiner, C. J., & Van De Bund, W. (2015). The use of remote sensing to characterise hydromorphological properties of European rivers. <https://doi.org/10.1007/s00027-015-0430-7>
- Corenblit, D., Steiger, J., Gurnell, A. M., Tabacchi, E., & Roques, L. (2009). Control of sediment dynamics by vegetation as a key function driving biogeomorphic succession within fluvial corridors. *EARTH SURFACE PROCESSES AND LANDFORMS Earth Surf. Process. Landforms*, 34, 1790–1810. <https://doi.org/10.1002/esp.1876>
- Coburn, C. A., Smith, A. M., Logie, G. S., & Kennedy, P. (2018). Radiometric and spectral comparison of inexpensive camera systems used for remote sensing. *International Journal of Remote Sensing*, 39(15–16), 4869–4890. <https://doi.org/10.1080/01431161.2018.1466085>
- Dietrich, J. T. (2016). Riverscape mapping with helicopter-based Structure-from-Motion photogrammetry. *Geomorphology*, 252, 144–157. <https://doi.org/10.1016/J.GEOMORPH.2015.05.008>
- Dietrich, J. T. (2017). Bathymetric structure-from-motion: extracting shallow stream bathymetry from multi-view stereo photogrammetry. *Earth Surface Processes and Landforms*, 42(2), 355–364.
- Federal Aviation Administration. (2014). FAA Fact Sheet—Small Unmanned. "Regulations (Part 107)." FAA: Washington, DC, USA

- Fonstad, M. A., Dietrich, J. T., Courville, B. C., Jensen, J. L., & Carbonneau, P. E. (2013). Topographic structure from motion: a new development in photogrammetric measurement. *Earth Surface Processes and Landforms*, 38(4), 421–430. <https://doi.org/10.1002/esp.3366>
- Galiatsatos, N., Donoghue, D. N., Knox, D., & Smith, K. (2007, July). Radiometric normalisation of multisensor/multitemporal satellite images with quality control for forest change detection. In 2007 International Workshop on the Analysis of Multi-temporal Remote Sensing Images (pp. 1-6). IEEE.
- González, E., Sher, A. A., Tabacchi, E., Masip, A., & Poulin, M. (2015). Restoration of riparian vegetation: A global review of implementation and evaluation approaches in the international, peer-reviewed literature. *Journal of Environmental Management*, 158, 85–94. <https://doi.org/10.1016/J.JENVMAN.2015.04.033>
- Göthe, E., Timmermann, A., Januschke, K., & Baattrup-Pedersen, A. (2016). Structural and functional responses of floodplain vegetation to stream ecosystem restoration. *Hydrobiologia*, 769(1), 79–92. <https://doi.org/10.1007/s10750-015-2401-3>
- Hough-Snee, N., Roper, B. B., Wheaton, J. M., Budy, P., & Lokteff, R. L. (2013). Riparian vegetation communities change rapidly following passive restoration at a northern Utah stream. *Ecological Engineering*, 58, 371-377.
- Janssen, P., Piégay, H., Pont, B., & Evette, A. (2019). How maintenance and restoration measures mediate the response of riparian plant functional composition to environmental gradients on channel margins: Insights from a highly degraded large river. *Science of The Total Environment*, 656, 1312–1325. <https://doi.org/10.1016/j.scitotenv.2018.11.434>
- Jeong, S. G., Mo, Y., Kim, H. G., Park, C. H., & Lee, D. K. (2016). Mapping riparian habitat using a combination of remote-sensing techniques. *International Journal of Remote Sensing*, 37(5), 1069–1088. <https://doi.org/10.1080/01431161.2016.1142685>
- Kalny, G., Laaha, G., Melcher, A., Trimmel, H., Weihs, P., & Rauch, H. P. (2017). The influence of riparian vegetation shading on water temperature during low flow conditions in a medium sized river. *Knowledge & Management of Aquatic Ecosystems*, (418), 5. <https://doi.org/10.1051/kmae/2016037>
- Kondolf, G. M. (1997). Hungry water: Effects of dams and gravel mining on river channels. *Environmental Management*, 21(4), 533–551.
- Knighton, D. (1998). *Fluvial forms and processes: a new perspective*. Routledge.
- Lyons, J., S. Trimble, & L. Paine. 2000. Grass versus trees: Managing riparian areas to benefit streams of central North America. *Journal of the American Water Resources Association* DOI: 10.1111/j.1752-1688.2000.tb04317.x

- Magilligan, F. J., & McDowell, P. F. (1998). Stream Channel Adjustments Following Removal of Cattle Grazing, *33*(4), 867–878.
- Marcus, W. A., & Fonstad, M. A. (2008). Optical remote mapping of rivers at sub-meter resolutions and watershed extents. *Earth Surface Processes and Landforms*, *33*, 4–24. <https://doi.org/10.1002/esp.1637>
- Marteau, B., Vericat, D., Gibbins, C., Batalla, R. J., & Green, D. R. (2017). Application of Structure-from-Motion photogrammetry to river restoration. *Earth Surface Processes and Landforms*, *42*(3), 503–515. <https://doi.org/10.1002/esp.4086>
- Mathews, A. J. (2015). A Practical UAV Remote Sensing Methodology to Generate Multispectral Orthophotos for Vineyards. *International Journal of Applied Geospatial Research*, *6*(4), 65–87. <https://doi.org/10.4018/ijagr.2015100104>
- McDowell, P. F., & Magilligan, F. J. (1997). Response of stream channels to removal of cattle grazing disturbance: Overview of western US exclosure studies. *Manage, et of Landscapes Disturbed by Channel Incision*, (Part 2), 1–7.
- Michez, A., Piégay, H., Lisein, J., Claessens, H., & Lejeune, P. (2016). Classification of riparian forest species and health condition using multi-temporal and hyperspatial imagery from unmanned aerial system. *Environmental Monitoring and Assessment*, *188*(3), 1–19. <https://doi.org/10.1007/s10661-015-4996-2>
- Middle Fork IMW Working Group. 2017. Middle Fork John Day River Intensively Monitored Watershed Final Summary Report.
- Muller, I., M. Delisle, M. Ollitrault, & I. Bernez. 2015. Responses of riparian plant communities and water quality after 8 years of passive ecological restoration using a BACI design. *Hydrobiologia*. DOI: 10.1007/s10750-015-2349-3
- Nijland, 2012. Basics of Infrared Photography, Infrared light (2012).Web. [http://www.ir-photo.net/ir\\_imaging.htm](http://www.ir-photo.net/ir_imaging.htm)
- NW Power & Conservation Council. (2016). Fiscal year 2016 annual report: the state of the Columbia River Basin. *Report*, *1*, 2014-01.
- Palmer, M. A., Bernhardt, E. S., Allan, J. D., Lake, P. S., Alexander, G., Brooks, S., ... Sudduth, E. (2005). Standards for ecologically successful river restoration. *Journal of Applied Ecology*, *42*(2), 208–217. <https://doi.org/10.1111/j.1365-2664.2005.01004.x>
- Passalacqua, P., Belmont, P., Staley, D. M., Simley, J. D., Arrowsmith, J. R., Bode, C. A., ... Wheaton, J. M. (2015). Analyzing high resolution topography for advancing the understanding of mass and energy transfer through landscapes: A review. *Earth-Science Reviews*, *148*, 174–193. <https://doi.org/10.1016/j.earscirev.2015.05.012>



- Perucca, E., Camporeale, C., & Ridolfi, L. (2007). Significance of the riparian vegetation dynamics on meandering river morphodynamics. *Water Resources Research*, 43(3). <https://doi.org/10.1029/2006WR005234>
- Roni, P., Beechie, T. J., Bilby, R. E., Leonetti, F. E., Pollock, M. M., & Pess, G. R. (2002). A Review of Stream Restoration Techniques and a Hierarchical Strategy for Prioritizing Restoration in Pacific Northwest Watersheds. *North American Journal of Fisheries Management*, 22(1), 1–20. [https://doi.org/10.1577/15488675\(2002\)022<0001:AROSRT>2.0.CO;2](https://doi.org/10.1577/15488675(2002)022<0001:AROSRT>2.0.CO;2)
- Roni, P., Åberg, U., & Weber, C. (2018). A Review of Approaches for Monitoring the Effectiveness of Regional River Habitat Restoration Programs. *North American Journal of Fisheries Management*, 38(5), 1170–1186. <https://doi.org/10.1002/nafm.10222>
- Rosgen, D., Taillacq, A., Rosgen, B., & Geenen, D. (2018). A Technical Review of the Columbia Habitat Monitoring Program’s Protocol, Data Quality. Retrieved from <https://www.cbfish.org/Document.mvc/Viewer/P159913>
- Rumps, J. M., Katz, S. L., Barnas, K., Morehead, M. D., Jenkinson, R., Clayton, S. R., & Goodwin, P. (2007). Stream Restoration in the Pacific Northwest: Analysis of Interviews with Project Managers. *Restoration Ecology*, 15(3), 506–515. <https://doi.org/10.1111/j.1526-100X.2007.00246.x>
- Smith, G. M., & Milton, E. J. (1999). The use of the empirical line method to calibrate remotely sensed data to reflectance. *International Journal of remote sensing*, 20(13), 2653-2662.
- Strahler, A.H. 1980. The Use of Prior Probabilities in Maximum Likelihood Classification of Remotely Sensed Data. *Remote Sensing of Environment*, Vol. 10, pp. 429-441.
- Tucker, C.J. (1979) Red and Photographic Infrared Linear Combinations for Monitoring Vegetation, *Remote Sensing of Environment*, **8(2)**,127-150.
- U.S. Forest Service (2012) Stream Inventory Handbook Levels I and II, Pacific Northwest Region, Version 2.12, Region 6.
- Vázquez-Tarrío, D., Borgniet, L., Liébault, F., & Recking, A. (2017). Using UAS optical imagery and SfM photogrammetry to characterize the surface grain size of gravel bars in a braided river (Vénéon River, French Alps). *Geomorphology*, 285, 94–105. <https://doi.org/10.1016/j.geomorph.2017.01.039>

- Wang, C., & Myint, S. (2015). A Simplified Empirical Line Method of Radiometric Calibration for Small Unmanned Aircraft Systems-Based Remote Sensing. *IEEE Journal of Selected Topics in Applied Earth Observations and Remote Sensing*, 8(5), 1876-1885. [7098353]. <https://doi.org/10.1109/JSTARS.2015.2422716>
- Watanabe, Y., & Kawahara, Y. (2016). UAV photogrammetry for monitoring changes in river topography and vegetation. *Procedia Engineering*, 154, 317–325. <https://doi.org/10.1016/j.proeng.2016.07.482>
- Winward, A. H. (2000). Monitoring the vegetation resources in riparian areas. RMRS-GTR-47. Ogden, UT: US Department of Agriculture, Forest Service, Rocky Mountain Research Station. 49 p., 47.
- Wolman, M. G., A method of sampling coarse river-bed material, *Am. Geophys. Union Trans.* 35, 951-956, 1954.
- Woodget, A. S., Austrums, R., Maddock, I. P., & Habit, E. (2017). Drones and digital photogrammetry: from classifications to continuums for monitoring river habitat and hydromorphology. *Wiley Interdisciplinary Reviews: Water*, 4(4), e1222. <https://doi.org/10.1002/wat2.1222>
- Woodget, A. S., Carbonneau, P. E., Visser, F., & Maddock, I. P. (2015). Quantifying submerged fluvial topography using hyperspatial resolution UAS imagery and structure from motion photogrammetry. *Earth Surface Processes and Landforms*, 40(1), 47–64. <https://doi.org/10.1002/esp.3613>
- Zhou, L., Tucker, C. J., Kaufmann, R. K., Slayback, D., Shabanov, N. V., & Myneni, R. B. (2001). *Variations in northern vegetation activity inferred from satellite data of vegetation index during 1981 to 1999. JOURNAL OF GEOPHYSICAL RESEARCH* (Vol. 106). <https://doi.org/10.1029/2000JD000115>